The Effect of Thermal Cycles on Mechanical Properties of 3D-Printed Dental Aligners Incorporating Long Optical Glass Fibers

Gao Xiyuan Jack

LKS Faculty of Medicine, The University of Hong Kong

Supervised by Professor Dan Kiho Cho

Faculty of Dentistry, The University of Hong Kong

Laidlaw Undergraduate Research and Leadership Programme

Abstract

The growing demand for aesthetic orthodontic treatment has accelerated the adoption of 3D-printed clear aligners. At the same time, the limitations of 3D-printed aligners, such as elastic deformation and poor fatigue resistance, have led to the technique of reinforcing fibers into aligners. However, the mechanical properties of the material have not been fully understood. This study aims to investigate the effects of long optical glass fiber reinforcement on the properties of 3D-printed TC85 resin aligners under simulated intraoral aging conditions. The specimens were divided into two groups either with fiber or without fiber. Within the two groups, specimens were further divided based on thermal cycling as control, 500 cycles, and 1000 cycles. This helps to evaluate color stability (ΔE), surface roughness (Ra), elastic modulus, and ultimate tensile strength (UTS) of specimens. Statistical analysis was performed through one-way ANOVA with Tukey's post hoc test ($\alpha = 0.05$). Generally speaking, fiber-reinforced specimens exhibited significantly higher elastic modulus of 2.6-3 times and increased 42-48% UTS in comparison with unreinforced groups. Thermal cycling increased the surface roughness of aligners despite the presence of fiber but had minimal impact on mechanical properties. Color stability somehow decreased with cycling, which may require further investigation. The result of this study provides an understanding of the mechanical properties of 3D-printed aligners incorporating glass fiber through thermal cycling, which can be used to support future aligner therapy in orthodontics.

Keywords: Clear Aligners, 3D-printing, Embedded Optical Glass Fiber, Thermocycling, Mechanical Properties, Orthodontics

Table of Contents

Introduction

The increasing demand for aesthetically pleasing orthodontic treatments has driven significant advancements in the development of clear aligner therapy over conventional fixed appliances (Tartaglia et al., 2021). Economic trends have predicted that the market size for clear aligners will grow 13% from USD 3.1 billion in 2021 to USD 11.6 billion in 2027. While the majority of clear aligners are manufactured using thermoformed plastic materials such as polyethylene terephthalate glycol (Bichu et al., 2022). Although these materials demonstrated clinical standards but inherent mechanical limitations of restricted elastic deformation and suboptimal fatigue resistance, which often necessitate increased material thickness to ensure durability at the expense of patient comfort (Dalaie et al., 2021). Recent developments in 3D printing have emerged as a suitable alternative for thermoplastic materials, specifically using photocurable resin of TC-85 (Niu et al., 2024). Unlike conventional thermoforming techniques, 3D printing enables precise dimensional control and has better trueness with accuracy. This allows the aligner to apply more effective orthodontic forces and consistent tooth movement (Maniukakis et al., 2024). To further enhance the mechanical deficiencies, the incorporation of long optical glass fibers into the resin aligner has been seen as a promising strategy. Studies have shown that the embedment of reinforcement elements will enhance the structural performance of tensile strength, elastic modulus, fatigue resistance, and thermal stability compared to unreinforced 3D-printed aligners (Lee et al., 2022). Recent academic reviews of 3D-printed dental materials have focused primarily on the biocompatibility testing presented in ISO 10993 (Vas and Jain, 2024). However, the mechanical properties along with long-term performance characteristics of the TC-85 material under clinically relevant repeated intraoral thermocycling conditions remain insufficiently characterized. This regulatory gap highlights the importance of studying the mechanical retention of these new materials in simulated oral environments. As a result, this study aims to present a comprehensive investigation of the mechanical properties of 3D-printed aligners using TC-85 material incorporating long optical glass fibers. The findings of this research study will establish quantitative relationships between thermal cycling and mechanical

properties retention, ranging from tensile strength, elastic modulus, surface roughness, to color stability, which provide a scientific framework for developing next-generation aligner systems.

Materials and Methods

Specimen Preparation

A transparent dental resin TC-85DAC (Graphy, Korea) was used as the fundamental material, mainly due to its enhanced mechanical properties and biocompatibility. To optimize performance, polyimide-coated optical glass fibers (DK Photonics Ltd, China) with an average diameter of 156 μm were embedded into the resin matrix. All fibers underwent the cleaning process, where it is mechanically agitated using a Vortex mixer (Jeio Tech Co., Ltd, Korea). Specifically, acetone was used for initial cleaning for the removal of organic residues, followed by rinsing with deionized water to eliminate solvent traces. Fibers were then oven-dried at 100°C for 60 minutes to ensure complete moisture and contaminants removal before further characterization. In this research, all specimens followed a dumbbell shape of 70 mm x 10 mm x 1 mm compliant with ISO 527-1:2019(E) in Figure 1a. for mechanical properties experiments and were 3D printed using Sonic Mini 8 K printer with a 405 nm blue-violet light LCD technology (Phrozen Technology, Taiwan). To accommodate the embedment of glass fiber, a rectangular cavity of 25 mm x 0.22 mm x 0.22 mm in Figure 1b. was incorporated at the center of the specimen during the design process. Specimen Geometries were designed using Blender and exported in Standard Tessellation Language (STL) format. The STL files were then processed in Chitubox_Basic (Shenzhen CBD Technology Co., China) for slicing and support structure generation in Figure 1c. A thickness of 1 mm was maintained across all specimens to ensure there were no thickness-related variations for uniformity. For specimens with fibers, the printer was paused at the 203rd layer corresponding to the cavity height, allowing for manual insertion of the pre-cleaned glass fiber. The specimens were then partially cured using Bluephase Style (Ivoclar Ltd., Liechtenstein) with 1100 mW light output to the fiber being

embedded and not filling out once the rest of the printing process resumed. All specimens are washed using 95% isopropyl alcohol to remove liquid resin on the surface. Non-reinforced specimens will then be post-cured for 30 minutes, while fiber-reinforced specimens are being post-cured for 60 minutes to ensure complete resin polymerization using a UV curing chamber (ARUM Dentistry, Korea). A total of 30 specimens were printed, consisting of 15 fiber-reinforced and 15 non-fiber-reinforced **(Appendix A: Experimental Equipment).**

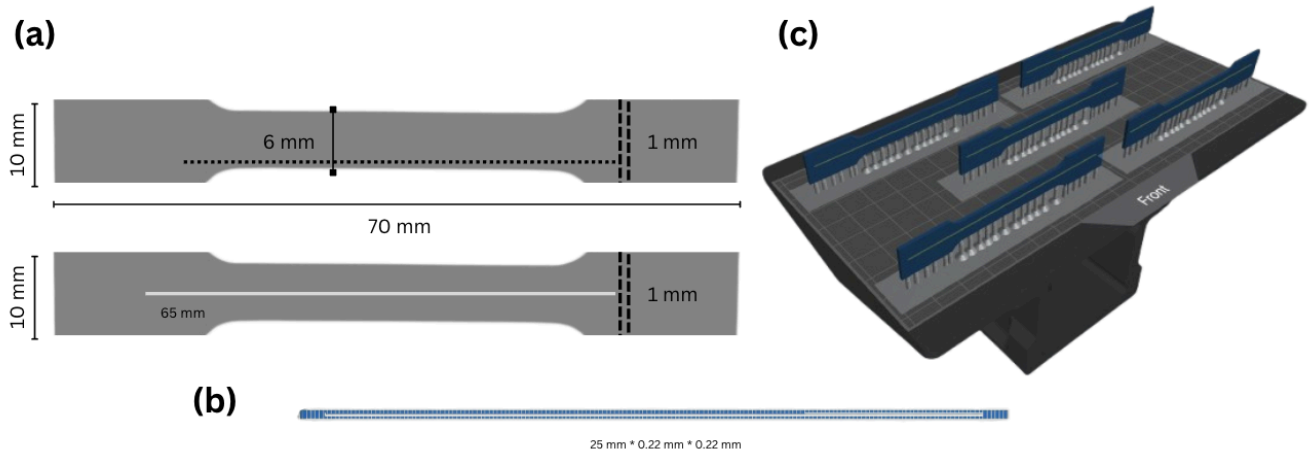

Figure 1 **(a)** Dumbbell Shape Specimen Dimensions. **(b)** Rectangular Cavity for Embedding Fiber. **(c)** 3D-Printing Layout in Chitubox_Basix. with Support

Experimental Protocol

Thermal Cycling to Stimulate Aging

The 30 specimens were further divided into three subgroups for the thermal cycling procedure shown in Table 1. According to ISO 11405 of the dental material aging testing protocol, the thermal cycling machine was maintained between temperature ranges of 5°C for cold and 55°C for hot baths of deionized water **(Appendix A: Experimental Equipment)**. The established aging protocol is designed for 500 and 1000 cycles of thermal cycling to simulate 7 and 14 days of clinical usage respectively. Each cycle

consisted of 20 seconds dwell times in both cold and hot water and 14 seconds of transfer interval between the baths, measured with digital counters (CT6S-1P2, United States).

Table 1 Experimental Group Distribution of 30 Printed Specimens

Group	Type of Specimens
Control (10 Specimens)	Fiber-Reinforced - 5 specimens without thermocycle Non-Reinforced - 5 specimens without thermocycle
500 Cycle (10 Specimens)	Fiber-Reinforced - 5 specimens 500 thermocycle Non-Reinforced - 5 specimens 500 thermocycle
1000 Cycle (10 Specimens)	Fiber-Reinforced - 5 specimens 1000 thermocycle Non-Reinforced - 5 specimens 1000 thermocycle

Optical Characterization

Specimens (n=4 per group) both fiber-reinforced and non-reinforced, are measured with the Nix Pro 2 color sensor (Nix, Canada) to analyze the effect of thermocycling on color change based on ISO 7724-3. Specifically, each specimen was measured at three different points to ensure the relevance and significance of the color change. The sensor contains a built-in lens and tristimulus colorimeter to capture light reflected from the surface. The analog color is converted into CIELAB digital values defined by CIE of L* for lightness, a* and b* for the chromaticity of red-green or blue-yellow. These values are used to calculate ΔE* for color change as described by the following equation:

$$\Delta E^{*} = \sqrt{\Delta L^{*2} + \Delta a^{*2} + \Delta b^{*2}}$$

where ΔL*, Δa*, and Δb* are the values from each aged group subtracting the control group.

Surface Characterization

Surface roughness was measured using atomic force microscopy (Bruker Corporation, USA) in peak-force tapping mode. Only fiber-reinforced specimens (n=1 per group) with ten 10 x 10 μm² scan areas were selected, as embedding fiber generally does not change surface roughness (Alshammari et al., 2025). The specimens were used to determine surface roughness (R_a) and were calculated using NanoScope Analysis software, with both 2D and 3D diagrams being captured for clinical presentation.

Tensile Strength with Elastic Modulus

Tensile properties were evaluated for all groups and types of standardized dumbbell-shaped specimens (n=4 per group). Testing was performed using an Instron ElectroPuls E3000 universal testing machine (Norwood, USA) under laboratory conditions of 25°C ± 2°C and humidity of 50% ± 5% with a constant crosshead speed of 5mm/min **(Appendix A: Experimental Equipment)**. During the test, deformation was continuously monitored, and the apparatus recorded synchronized force displacement data until the specimen fracture occurred. The result outlined the data for extension (mm) and load (N), which are used to calculate tensile strain and stress by the following formula:

$$\sigma = \frac{F}{A_0} \qquad \epsilon = \frac{\Delta L}{L_0}$$

where σ (MPa) represents stress with F and A_0 as applied force (N) and original cross-sectional area (mm^2) respectively. ϵ is the strain and ΔL is extension (mm) with L_0 showing the original length (mm). Stress-strain curves were generated using tensile strain and stress resulting from calculations. Additionally, ultimate tensile strength (UTS) is identified as the peak stress value recorded before specimen fracture, and elastic modulus is determined as the slope of the linear elastic region of 0.05-0.30% strain from the stress-strain curves.

Data Collection

All testing data were systematically collected under controlled laboratory conditions using calibrated instrumentation. These data were analyzed in GraphPad Prism 10 software (San Diego, USA) after verifying normality and homogeneity of variance. One-way ANOVA with Tukey's HSD post hoc tests were then performed to compare specimens with the presence of fiber and not as well as thermocycling for color change, surface roughness, tensile strength with elastic modulus, and UTS. The significance threshold holds at $\alpha = 0.05$, and outliers were rechecked and excluded if artifactual.

Result

Optical Characterization of Color Change

The results from one-way ANOVA for the evaluation of thermal cycling on ΔE non-reinforced specimens are shown in Table 2. This revealed statistically significant effects of thermal cycling as ΔE indicated by the p-value, and explained 39.3% of the observed variation. The analysis was followed by a post hoc comparison between groups of specimens without fiber, as presented in Table 3. Together with the graphical result in Figure 2a., it is clear that both specimens that underwent 500 and 1000 cycles showed significantly higher discoloration than the non-cycled control. Surprisingly, the effect is most pronounced in the initial 500 cycles. However, the difference between 500 and 1000 cycles was not statistically significant, suggesting that the change in ΔE slows down, demonstrating a non-linear degradation pattern.

Table 2 Summarized ANOVA Results for Specimen Without Fiber

F-value	df	p-value	R^2
F = 10.76	(2, 33)	p = 0.0003	39.3%

Table 3 Pairwise Comparison to Assess Differences in ΔE Specimens Without Fiber

Comparison	Mean ΔE ($\pm$ SD)	p-value

Control vs. 500 cycles	15.83 ± 1.89 vs. 13.01 ± 0.91	p = 0.0002
Control vs. 1000 cycles	15.83 ± 1.89 vs. 13.88 ± 1.64	p = 0.010
500 vs. 1000 cycles	13.01 ± 0.91 vs. 13.88 ± 1.64	p = 0.357

A similar evaluation was performed to analyze the impact of thermal cycling on ΔE fiber-reinforced specimens, which are outlined in Table 4. The result indicated a statistically significant effect of thermal cycling but it is smaller in terms of effect size compared with non-reinforced specimens. Post-hoc comparison was followed as shown in Table 5. Based on the result in Figure 2b., only the 1000 cycle group showed significantly higher discoloration than the control while the 500 cycle group did not differ significantly unlike in non-reinforced specimens. However, the rate of ΔE The increase was smaller than non-reinforced specimens, suggesting fibers may mitigate degradation.

Table 4 Summarized ANOVA Results for Specimen With Fiber

F-value	**df**	**p-value**	**R^2**
F = 4.285	(2, 33)	p = 0.0022	20.6%

Table 5 Pairwise Comparison to Assess Differences in ΔE Specimens With Fiber

Comparison	**Mean ΔE ($\pm$ SD)**	**p-value**
Control vs. 500 cycles	16.50 ± 2.44 vs. 15.65 ± 1.14	p = 0.615
Control vs. 1000 cycles	16.50 ± 2.44 vs. 13.93 ± 2.68	p = 0.019
500 vs. 1000 cycles	15.65 ± 1.14 vs. 13.93 ± 2.68	p = 0.173

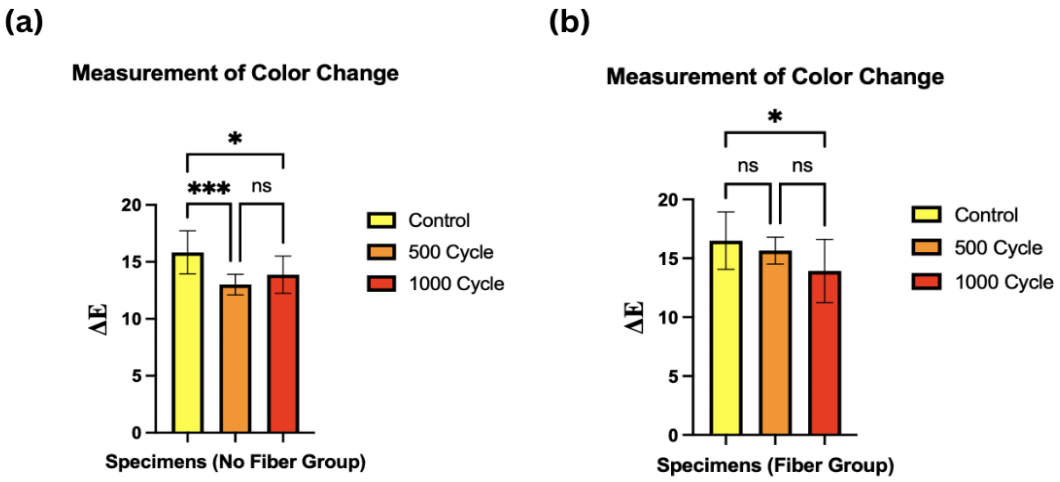

Figure 2. (a) Interleaved Bars of Mean with SD for Color Change in No Fiber Groups **(b)** Interleaved Bars of Mean with SD for Color Change in Fiber Groups

Surface Characterization of Roughness

The AFM result outlined a significant increase in surface roughness (R_a) after conducting thermal cycling, as shown in the result in Table 6 **(Appendix B: Visual Presentation of AFM Image).** Specifically, specimens in 500 and 1000 cycle groups exhibited nearly double the R_a value in comparison with the control group as shown in Table 7 and Figure 3 for graphical representation. While the change of roughness between 500 and 1000 cycle groups seems to have no progression, which may indicate that surface modifications occur primarily in the beginning stage of thermal cycling.

Table 6 Summarized ANOVA Results for Surface Roughness

F-value	**df**	**p-value**	**R^2**
F = 18.71	(2, 27)	p < 0.0001	58.08%

Table 7 Key Group Pairwise Comparison of Surface Roughness

Comparison	**Mean MPa [95% CI]**	**p-value**
Control vs. 500 Cycle	+0.101 [0.053 to 0.149]	p <0.0001

Control vs. 1000 Cycle	+0.103 [0.055 to 0.150]	p <0.0001
500 Cycle vs. 1000 Cycle	+0.0016 [-0.049 to 0.046]	NS

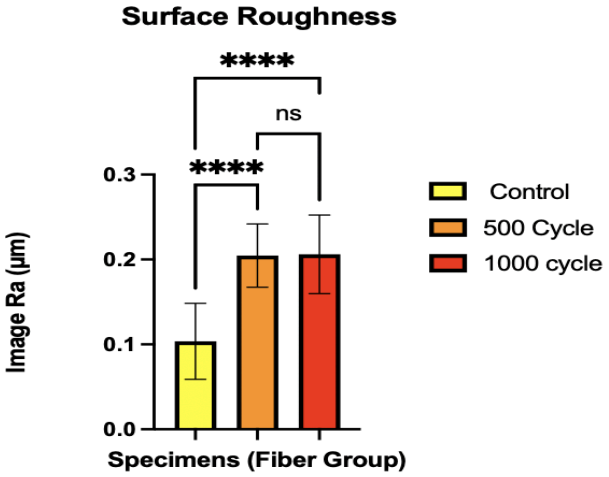

Figure 3. Interleaved Bars of Mean with SD for Surface Roughness Image R_a from AFM

Tensile Characterization of Elastic Modulus

The elastic modulus interpreted through tensile strength tests demonstrated profound differences between fiber and no fiber specimens, as shown with statistical results in Table 8 (**Appendix C: Display of Stress-Strain Curve)**. The presence of fiber is the dominant factor that influences elastic modulus, with all comparisons significant and a few key groups remain extremely significant as Table 9. Specifically in Figure 4. The fiber-reinforced groups showed approximately 2.6 to 3 times higher modulus of 475.9 to 542.6 MPa compared with the non-reinforced group of 178.7 to 229.2 MPa. However, thermal cycling does not seem to have a significant effect on elastic modulus for no fiber groups and only slightly increased modulus for fiber groups, both remain not significant.

Table 8 Summarized ANOVA Results for Elastic Modulus

F-value	**df**	**p-value**	**R^2**
F = 48.20	(5, 18)	p < 0.0001	93.05%

Table 9 Key Group Pairwise Comparison of Specimen With/Without Fiber

Comparison	Mean MPa (95% CI)	p-value
Control (no fiber) vs. Control (fiber)	-297.3 [-401.8 to -92.7]	p <0.0001
500 (no fiber) vs. 500 (fiber)	-258.6 [-363.1 to -154]	p <0.0001
1000 (no fiber) vs. 1000 (fiber)	-314.4 [-418.9 to -209.8]	p <0.0001

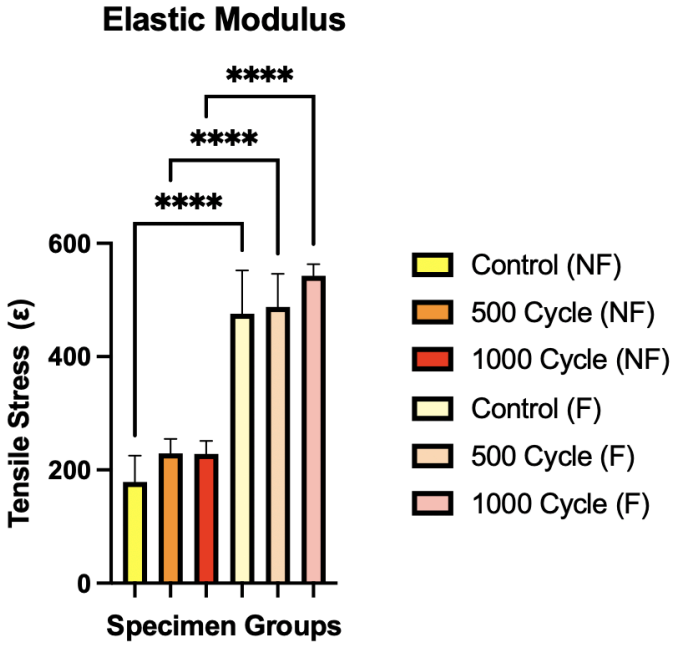

Figure 4. Interleaved Bars of Mean with SD for Elastic Modulus from UTS

Tensile Characterization of UTS

Similar to elastic modulus, the one-way ANOVA revealed extremely significant differences between groups as shown in Table 10 **(Appendix C: Display of Stress-Strain Curve).** The result showed an increase in UTS of approximately 42 to 48% across all conditions, for instance fiber specimen in the control group has a mean of 20.55 MPa compared to 11.77 MPa in the no fiber control group specimen with additional critical group comparison shown in Table 11 and Figure 5. While thermal cycling demonstrated minimal effects on UTS in all groups of specimens, indicating that the presence of fiber is the primary determinant for enhancing UTS.

Table 10 Summarized ANOVA Results for UTS

F-value	df	p-value	R^2
F = 47.63	(5, 18)	p < 0.0001	92.97%

Table 11 Key Group Pairwise Comparison of Specimen With/Without Fiber

Comparison	Mean MPa [95% CI]	p-value
Control (no fiber) vs. Control (fiber)	+8.78 [5.36 to 12.21]	p <0.0001
500 (no fiber) vs. 500 (fiber)	+9.29 [5.86 to 12.71]	p <0.0001
1000 (no fiber) vs. 1000 (fiber)	+10.59 [7.17 to 14.02]	p <0.0001

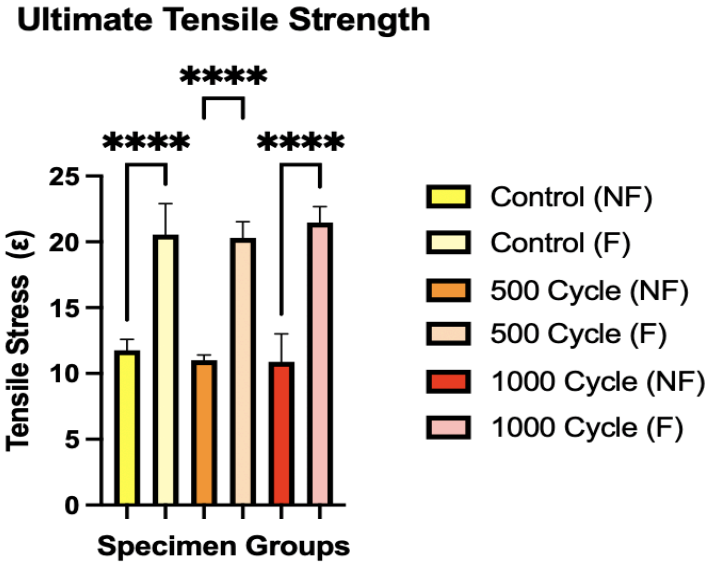

Figure 5. Interleaved Bars of Mean with SD for UTS

Discussion

This study systematically evaluated the effects of thermal cycling on the mechanical properties of 3D-printed aligners with and without optical glass fiber. The results show that the embedment of fiber potentially enhances its properties and reveals a mix of structure-property relationships while providing actionable insights for clinical practice.

Change in Color

Multiple studies have shown an increase in ΔE value in 3D-printed aligners after thermal cycling, stimulating intraoral conditions (Zhang et al., 2024). Although our findings contradicted the literature outlined a decreasing trend ΔE with more thermal cycles, meaning it potentially reduces visible color changes on the aligners. Despite the presence of fiber, both groups have the highest ΔE in the control specimens with decreasing discoloration after 500 and 1000 cycles respectively. The unexpected outcome may be due to stabilization effects during thermal cycling where surface irregularities or residual uncured monomers in the control group are reduced as a result of improving optical clarity, leading to less apparent color change (ŠimunoviĆ et al., 2024). However, there are some studies that state that the color stability of 3D-printed aligners depends heavily on the material formulation of the resin itself, combined with surface treatment and cycling protocols of the experiment (Koh et al., 2020). These comparative results suggest that color change does not necessarily end in a linear increase in discoloration; in fact, thermal cycling triggers complex chemical and physical changes within the material. Therefore, further research is required to fully understand the color change with thermal cycling.

Surface Roughness

Thermal cycling has significant effects on the 3D-printed aligner's surface roughness as supported by other studies (Zhang et al., 2024). While in both groups, roughness between 500 and 1000 groups showed minimal difference. Some findings have suggested a plateau effect in which thermal cycling causes expansion and microcracking in the early process, leading to a rougher surface. However, once initial damage progresses, further cycling induces relatively minor additional changes (Bhate et al., 2024). The results are essential for estimating the durability of clear aligner therapy in clinical practices, as greater surface roughness can potentially influence bacterial buildup and affect the overall aesthetic for patients.

Elastic Modulus

Similar to the literature, our experiment concludes that reinforcement of glass fiber significantly enhances the elastic modulus of the 3D-printed aligners. The fiber in a resin matrix acts as the

strengthening component to increase its stiffness and resistance to flexing (Miao et al., 2025). Although the elastic modulus has improved significantly between the fiber and the no fiber group specimens, the effect of thermal cycling is contradictory. Specifically, specimens in both groups exhibited an increase in elastic modulus after 500 and 1000 cycles. For fiber specimens, this may be attributed to the postcuring effect induced by thermal cycling, where additional crosslinking within the photopolymerized resin matrix enhances the density and stiffness. For non-fiber specimens, a similar post-curing effect may reduce molecular mobility and temporarily increase stiffness before degradation (Dalaie et al., 2021). This seems unusual, however, in clear aligner therapy, a lower modulus is more ideal during initial treatment to support patient comfort with the glass fiber gradually increasing in elastic modulus as continuous intraoral condition (Zhang et al., 2025). The outcome of the experiment is crucial in understanding the mechanical properties and clinical durability.

Ultimate Tensile Strength

Our result demonstrated significant improvement in UTS through the embedment of glass fiber along with thermocycling, which correlates with many other studies (Benal et al., 2023). Specifically, specimens without glass fiber displayed a decreasing trend in UTS as thermal cycling continued. This is potentially due to the accumulation of internal stresses and microcracking, as there is repeated expansion and contraction of material during thermal cycling. In comparison, specimens with fiber have much higher UTS as fiber improves load transfer and reduces porosity to strengthen the interface's crack resistance. Surprisingly, even with thermal cycling, UTS seems to have increased slightly in the 1000 cycle fiber group. This may be due to post-curing effects or improved fiber-matrix interfacial bonding during thermal cycling, since cycling itself potentially induces additional crosslinking in the polymer and releases residual stress making a tougher matrix surrounding the fiber. Additionally, it may also reduce porosity and increase interlaminar adhesion,leading to slightly increased UTS results shown in our experiment but after which a decrease in long-term fatigue performance dominates the mechanical

response (Muna et al., 2022). Thus, the incorporation of glass fiber can significantly enhance the aligner's UTS and be more resistant to usage in clinical settings.

Limitations and External Variables

To make the study result more representative, expanding of sample size is necessary as this study has a limited sample size of n=5 in each group which may reduce statistical power and limit the generalizability of the findings. Another modification should be made in the length of thermal cycling as 500 and 1000 cycles may not fully represent long-term clinical usage. Moreover is material variability since all specimens were 3D-printed which means there might be batch-to-batch differences in the resin, glass fiber, and time, and other external factors that influence results. For instance, some specimens may experience initial oxidation or environmental exposure before thermal cycling which contributed to abnormal color deviation. Potential human error in the experiment or measurement technique could also happen despite efforts to standardize the protocol.

Conclusion

This study provides a scientific foundation in understanding the mechanical properties of 3D-printed aligners. Thermal cycling somehow led to less color shift in aligners, while fibers did not disproportionately amplify the effects beyond their contributions. While surface roughness was significantly affected by thermal cycling, causing material degradation and a more uneven surface. Both elastic modulus and UST are significantly enhanced by the glass fiber while trends from thermal cycling can be observed but remain not significant. Potentially, incorporating optical glass fiber can enhance the aligner's mechanical properties. Future directions should focus on further evidence-based investigation to understand its clinical thresholds for advancement in clear aligner therapy.

Personal Reflection

Being selected as a Laidlaw Scholar working on a research project has been one of the most transformative experiences of my academic journey. As an undergraduate student, being given the opportunity to work in a lab is extremely valuable. I initially doubted my ability and whether research was for me as the challenges seemed insurmountable. I remember spending over a week just to print the specimen with multiple 3D printing failures, calibrating software, and testing different resin and printer settings. There were moments of frustration even despair when nothing worked despite the time spent. I learned the operation of different equipment such as 3D printers, UTM, AFM, etc and for the first time applied statistical theories from lectures to real data analysis. Looking back at it now, things that seemed impossible at first gradually became familiar through perseverance and the unwavering support of my supervisor and mentors. The technical skills I have gained are invaluable but personal growth matters more. I have become more resilient, confident in my ability to navigate uncertainty and at peace with the iterative nature of solving obstacles. Doing research has really taught me that mastery is not about instant success but about embracing the process and trusting that even if you fail, there is still a team rooting for you. I am sure these values will be carried with me beyond and become a better version of myself.

Acknowledgement

I would like to express my deepest gratitude to Professor Dan Kiho Cho for granting me the invaluable opportunity to pursue this research. I am also extremely thankful to Ching, Junjing, and Hong for their mentorship carried me through every stage of this journey. Their patient daily guidance in the laboratory, willingness to troubleshoot challenges with me, and teaching me technical skills. Not to forget the generous support of the Laidlaw Foundation and the University of Hong Kong for making this research project possible.

References

Alshammari, R. R., Alshihah, N., & Aldweesh, A. (2025). Quantitative evaluation of surface roughness and mass loss for different types of composite resins used for clear aligner attachments: an in vitro study. *Frontiers in Materials*, *12*. https://doi.org/10.3389/fmats.2025.1614811

Bhate, M., & Nagesh, S. (2024). Assessment of the effect of thermoforming process and simulated aging on the mechanical properties of clear aligner material. *Cureus*. https://doi.org/10.7759/cureus.64933

Bichu, Y. M., Alwafi, A., Liu, X., Andrews, J., Ludwig, B., Bichu, A. Y., & Zou, B. (2022). Advances in orthodontic clear aligner materials. *Bioactive Materials*, *22*, 384–403. https://doi.org/10.1016/j.bioactmat.2022.10.006

Dalaie, K., Fatemi, S. M., & Ghaffari, S. (2021a). Dynamic mechanical and thermal properties of clear aligners after thermoforming and aging. *Progress in Orthodontics*, *22*(1). https://doi.org/10.1186/s40510-021-00362-8

Dalaie, K., Fatemi, S. M., & Ghaffari, S. (2021b). Dynamic mechanical and thermal properties of clear aligners after thermoforming and aging. *Progress in Orthodontics*, *22*(1). https://doi.org/10.1186/s40510-021-00362-8

Koh, E., Cha, H., Kim, T., Ahn, J., & Lee, J. (2020). Color stability of three dimensional-printed denture teeth exposed to various colorants. *The Journal of Korean Academy of Prosthodontics*, *58*(1), 1. https://doi.org/10.4047/jkap.2020.58.1.1

Lee, S. Y., Kim, H., Kim, H., Chung, C. J., Choi, Y. J., Kim, S., & Cha, J. (2022). Thermo-mechanical properties of 3D printed photocurable shape memory resin for clear aligners. *Scientific Reports*, *12*(1). https://doi.org/10.1038/s41598-022-09831-4

Manoukakis, T., Nikolaidis, A. K., & Koulaouzidou, E. A. (2024). Polymerization kinetics of 3D-printed orthodontic aligners under different UV post-curing conditions. *Progress in Orthodontics*, *25*(1). https://doi.org/10.1186/s40510-024-00540-4

Miao, J.-T., Yang, B., Sang, X., Wu, L., & Ge, M. (2025). Interlayer Interface Reinforcement Strategy of glass fiber for preparing isotropic high-performance photocurable 3D printing polymer composites. *ScienceDirect*. https://www.sciencedirect.com/science/article/abs/pii/S1359835X25002489#:~:text=Meanwhile%2C%20modified%20GF%20(GF%2D,and%20expand%20their%20application%20fields

Muna, I. I., Mieloszyk, M., Rimasauskiene, R., Maqsood, N., & Rimasauskas, M. (2022). Thermal effects on mechanical strength of additive manufactured CFRP composites at stable and cyclic temperature. *Polymers MDPI*. https://pdfs.semanticscholar.org/5a28/b7356b64e479a722377b50dd47b2bf8f8651.pdf

Niu, C., Li, D., Zhang, Y., Wang, Y., Ning, S., Zhao, G., Ye, Z., Kong, Y., & Yang, D. (2024). Prospects for 3D-printing of clear aligners—a narrative review. *Frontiers in Materials*, *11*. https://doi.org/10.3389/fmats.2024.1438660

R, M. H., Benal, M. G. M., S, P. G., Tambrallimath, V., Ramaiah, K., Khan, T. M. Y., Bhutto, J. K., & Ali, M. A. (2023). Effect of short glass fiber addition on flexural and impact behavior of 3D printed polymer composites. *ACS Omega*, *8*(10), 9212–9220. https://doi.org/10.1021/acsomega.2c07227

Šimunović, L., Agović, S. Č., Marić, A. J., Bačić, I., Klarić, E., Uribe, F., & Meštrović, S. (2024). Color and chemical stability of 3D-Printed and thermoformed Polyurethane-Based aligners. *Polymers*, *16*(8), 1067. https://doi.org/10.3390/polym16081067

Tartaglia, G. M., Mapelli, A., Maspero, C., Santaniello, T., Serafin, M., Farronato, M., & Caprioglio, A. (2021). Direct 3D Printing of Clear Orthodontic Aligners: Current State and Future Possibilities. *MDPI*. https://www.mdpi.com/1996-1944/14/7/1799

Vas, N. V., & Jain, R. K. (2024). An Update on 3D-printed Orthodontic Aligners. *Journal of Clinical and Diagnostic Research*.

https://www.jcdr.net/articles/PDF/19279/67084_CE%5BRa1%5D_F(IS)_QC_Ref_Pat(SHK_OM)_PF1(VD_SS_OM)_PFA(KM)_PB(VD_OM)_PN(KM).pdf

Zhang, J., Zhang, Y., Tsoi, J., Yang, Y., & Cho, K. (2025). Static and dynamic mechanical properties of 3D-printed clear resin with embedded orthodontic metal wire. *ResearchGate*. https://www.researchgate.net/publication/390129291_Static_and_dynamic_mechanical_properties_of_3D-printed_clear_resin_with_embedded_orthodontic_metal_wire

Zhang, R., Zhao, L., Yu, L., & Tan, F. (2024). Influence of thermal-cycling or staining medium on the surface properties and color stability of conventional, milled, and 3D-printed base materials. *Scientific Reports*, *14*(1). https://doi.org/10.1038/s41598-024-80380-8

Appendix A: Experimental Equipment

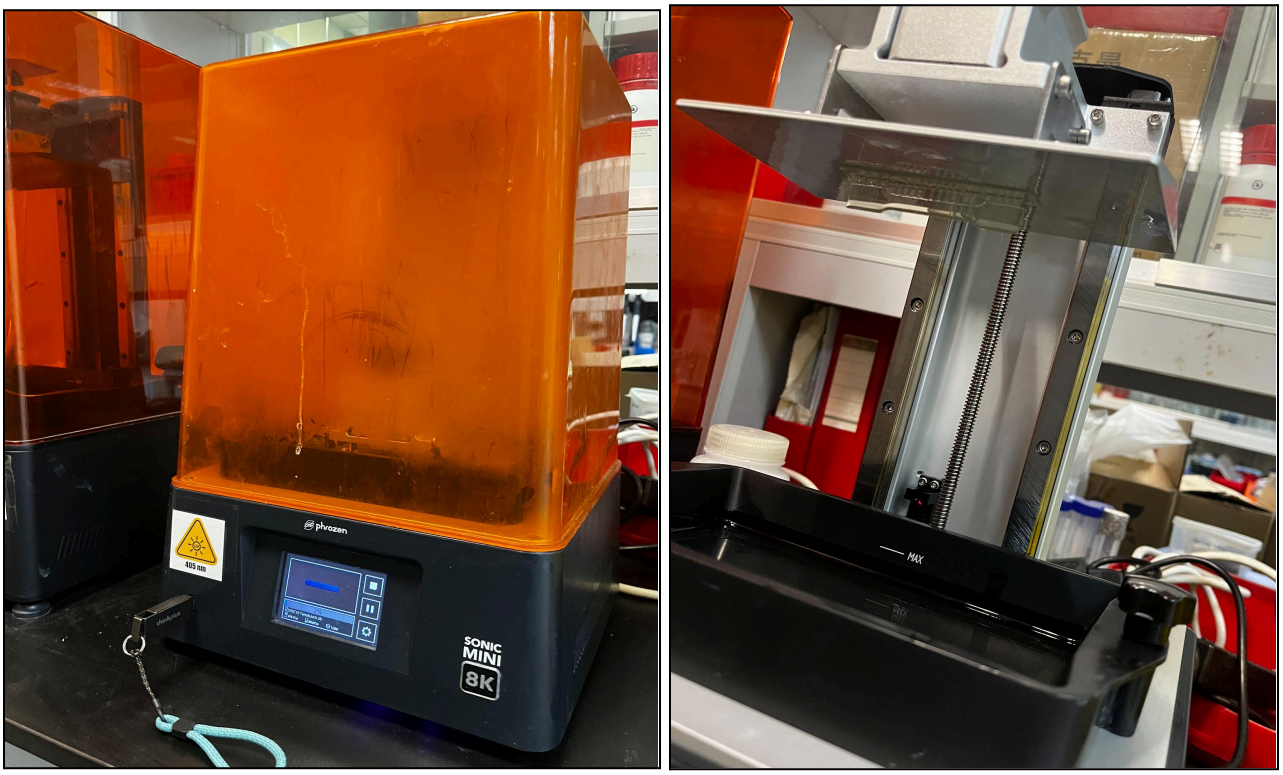

Display of Sonic Mini 8K Printer (Left) and Specimen Printing (Right)

UV Curing Chamber (Left) and Completed Specimen Display (Right)

Display of Thermal Cycling Machine

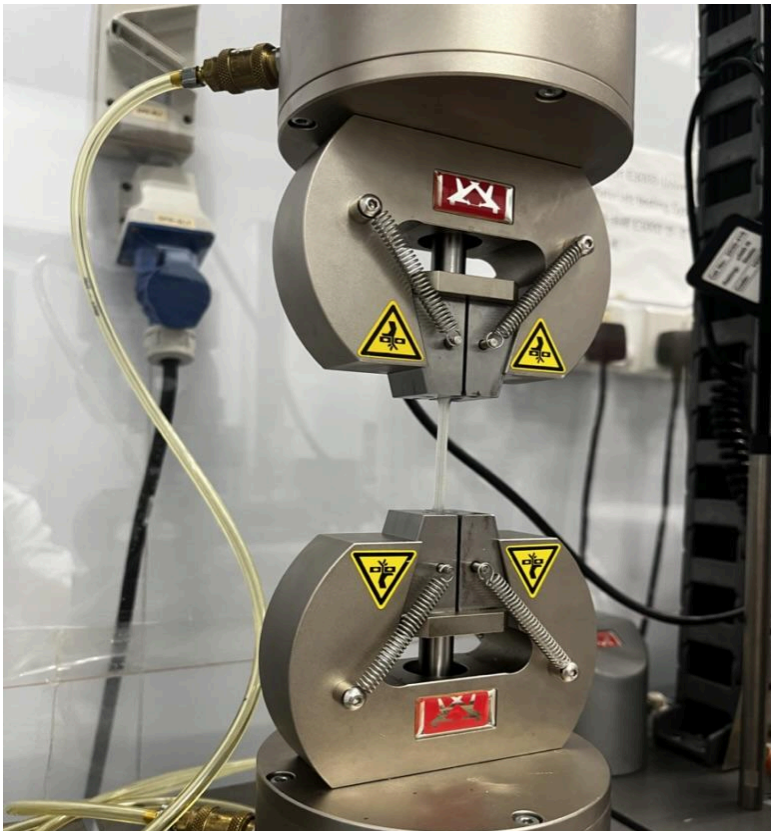

Display of Universal Testing Machine

Appendix B: Visual Presentation of AFM Images

Control Group

2D AFM Image **3D AFM Image**

(1)

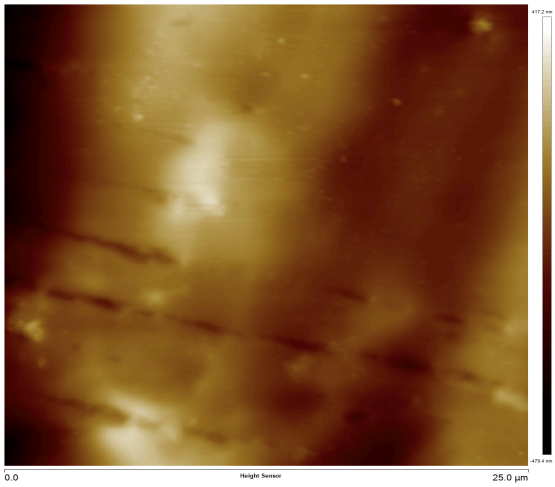

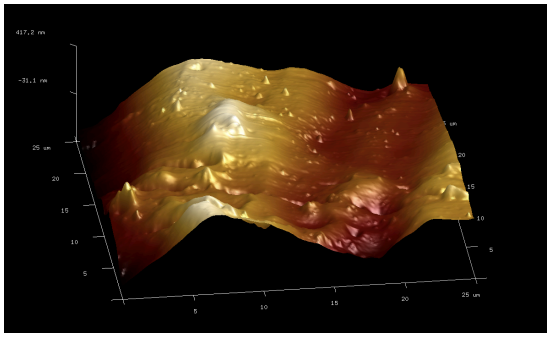

(2)

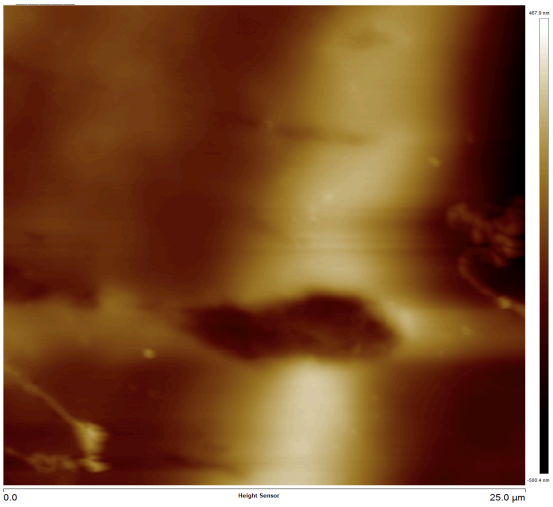

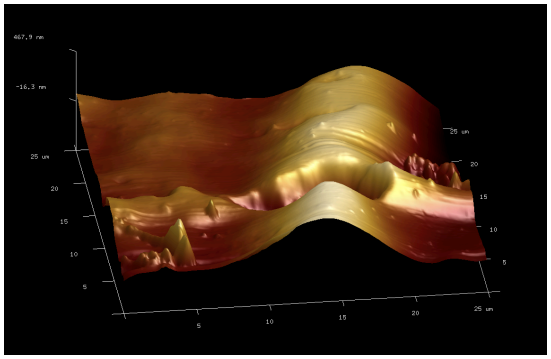

(3)

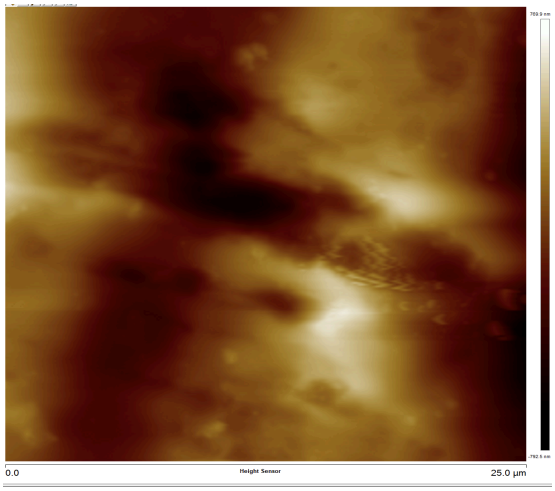

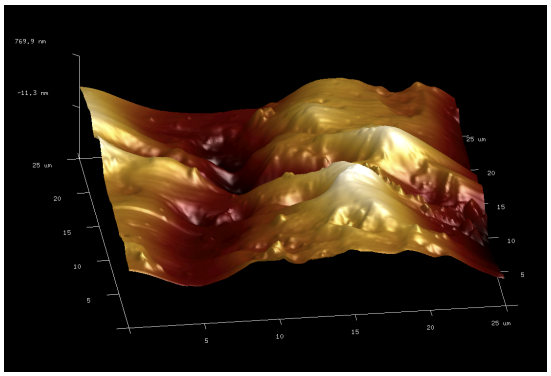

(4)

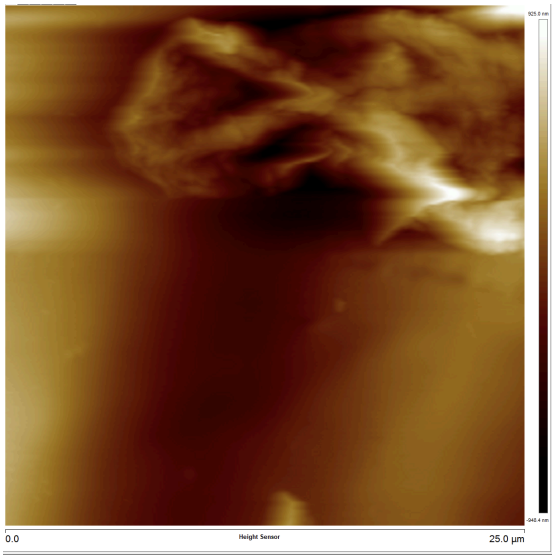
0.0
Height Sensor
25.0 µm

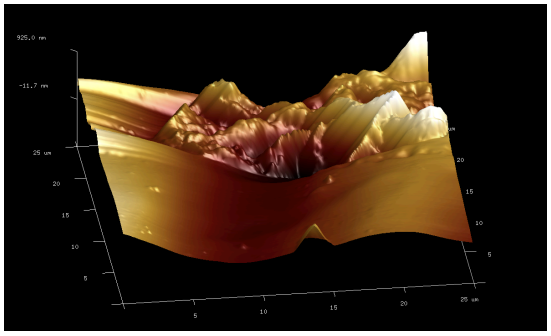
925.0 nm
-11.7 nm
25 um

(5)

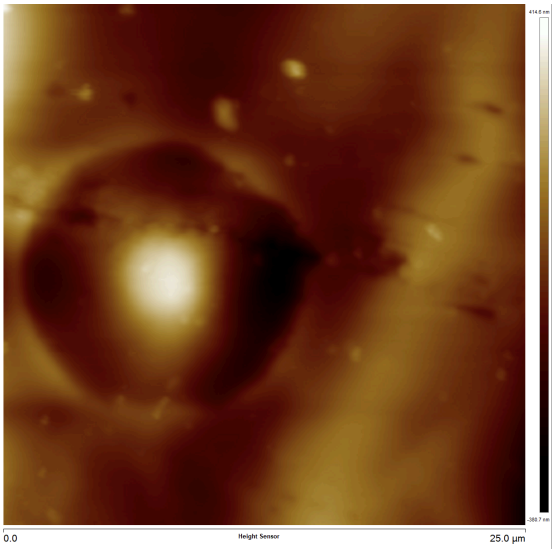
0.0
Height Sensor
25.0 µm

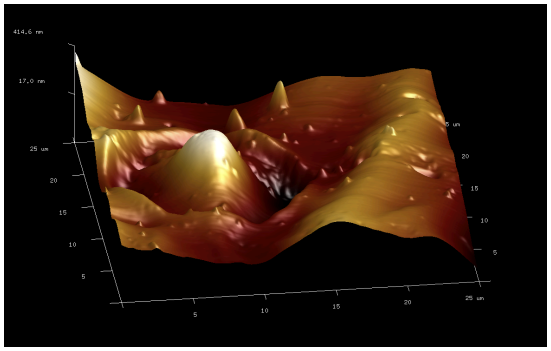
414.6 nm
17.0 nm
25 um

(6)

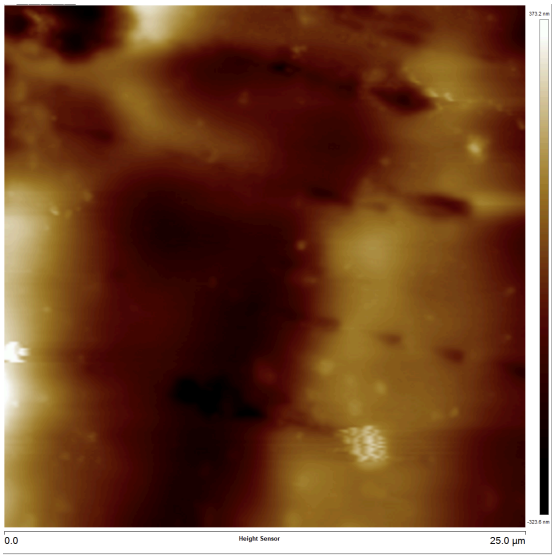
0.0
Height Sensor
25.0 µm

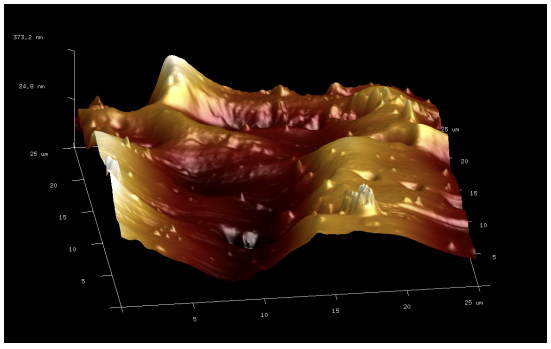
373.2 nm
24.0 nm
25 um

(7)

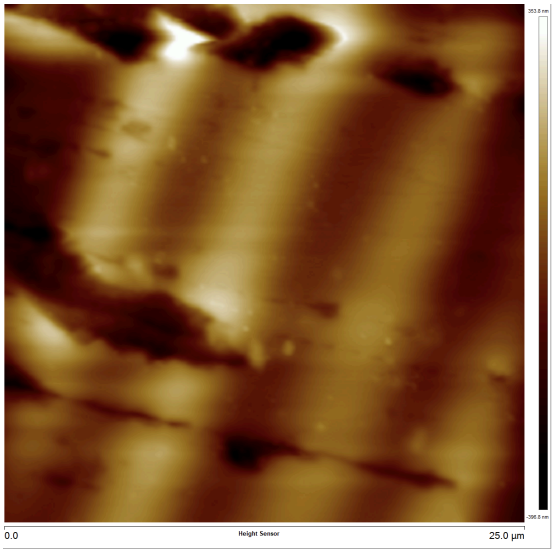
0.0
Height Sensor
25.0 µm

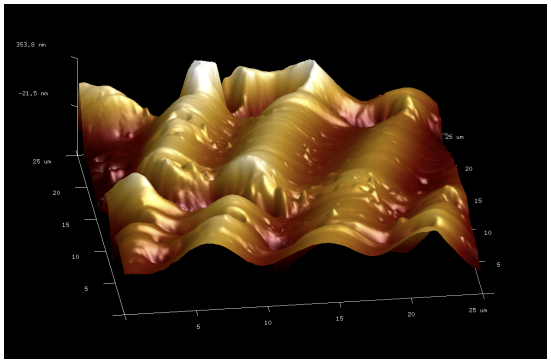

(8)

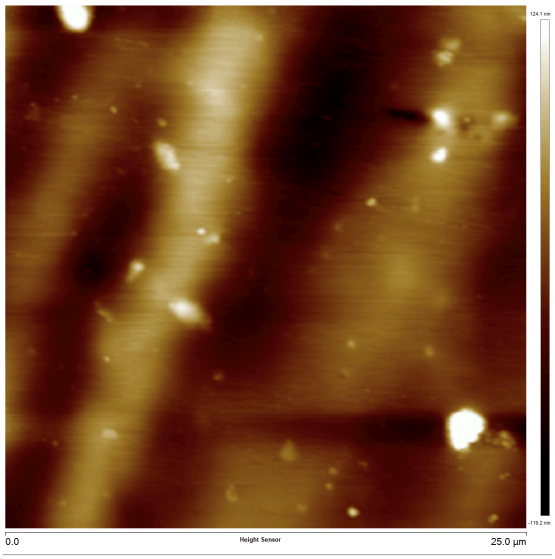
0.0
Height Sensor
25.0 µm

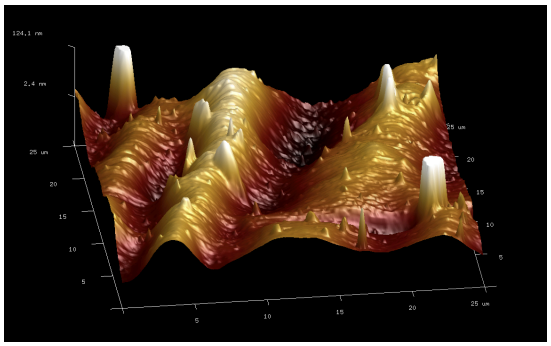

(9)

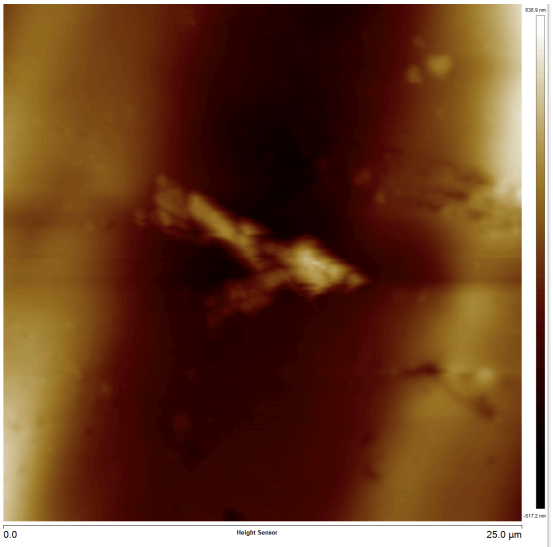
0.0
Height Sensor
25.0 µm

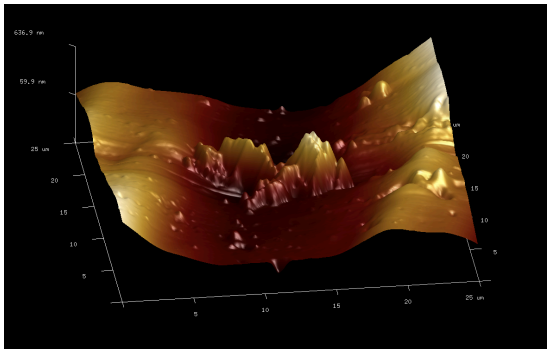

(10)

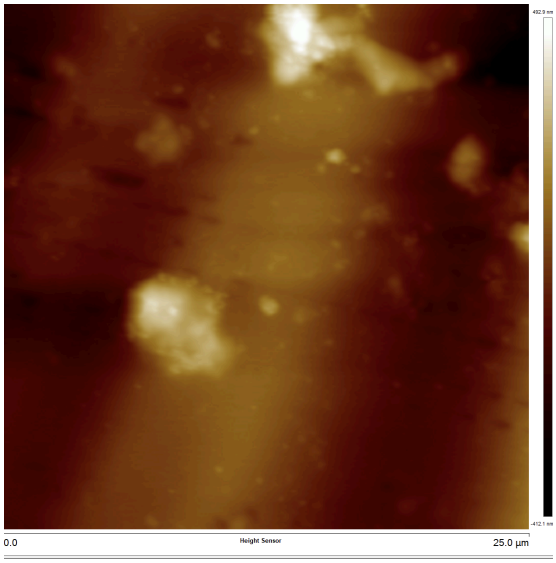

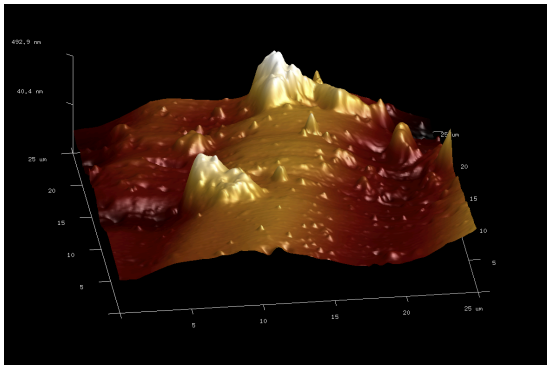

500 Cycle Group

2D AFM Image **3D AFM Image**

(1)

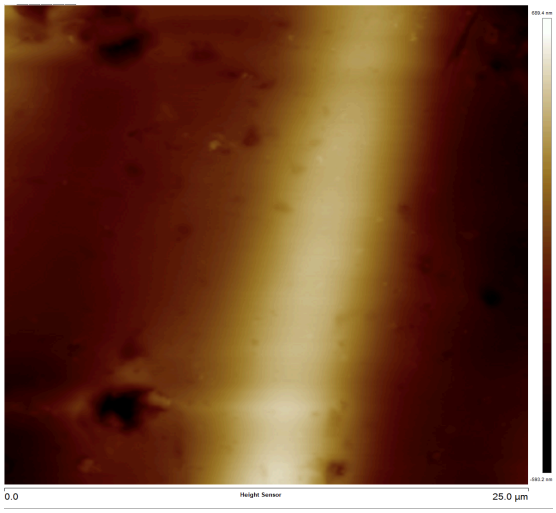

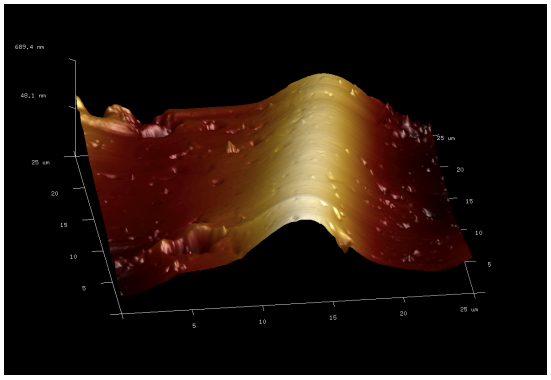

(2)

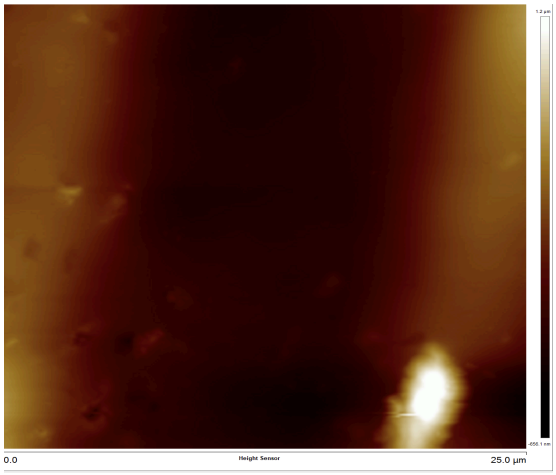

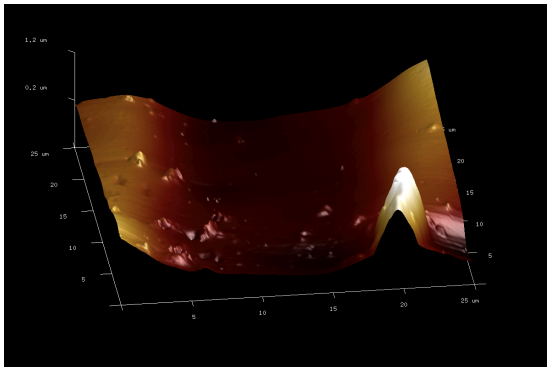

(3)

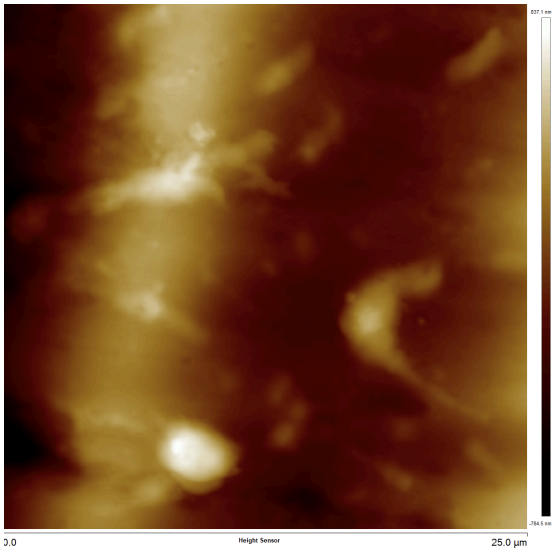
0.0
Height Sensor
25.0 µm

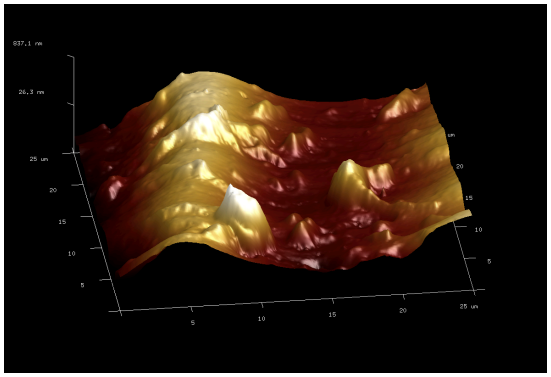

(4)

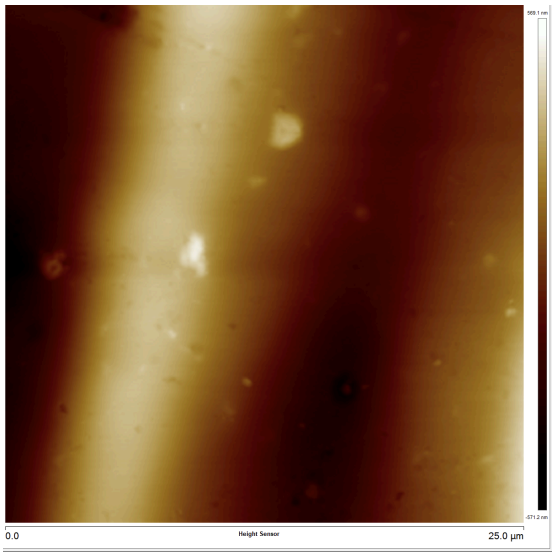
0.0
Height Sensor
25.0 µm

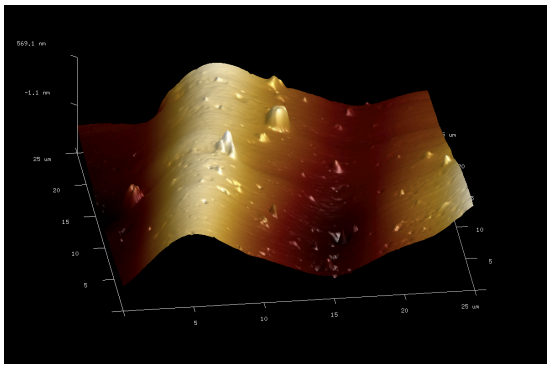

(5)

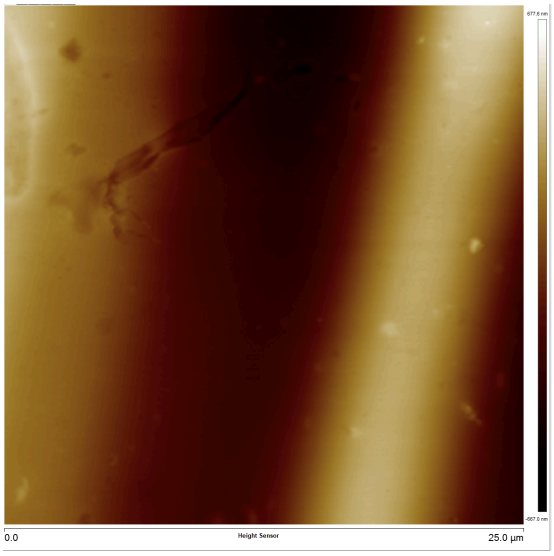
0.0
Height Sensor
25.0 µm

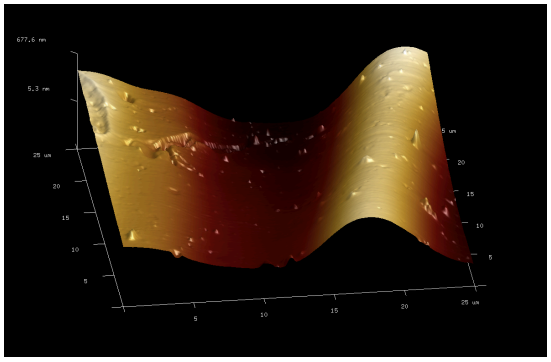

(6)

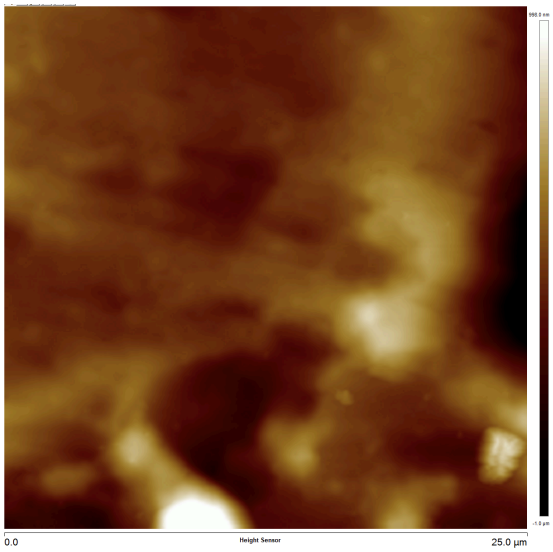
0.0
Height Sensor
25.0 µm

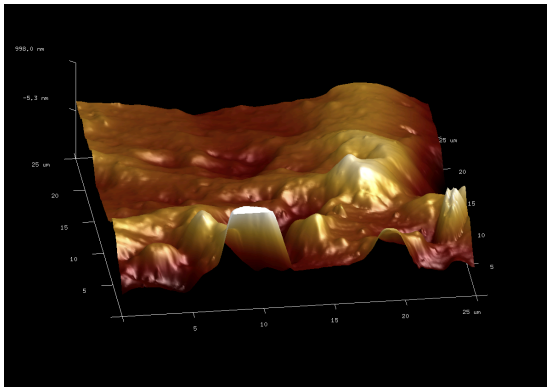

(7)

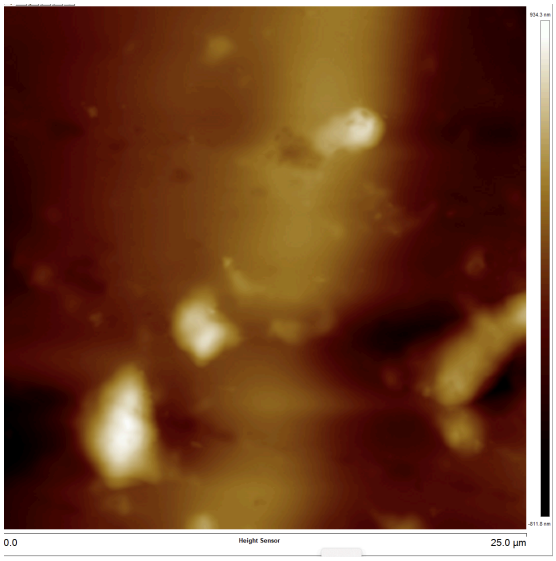
0.0
Height Sensor
25.0 µm

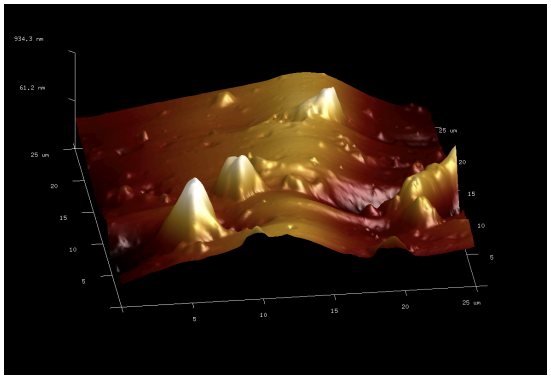

(8)

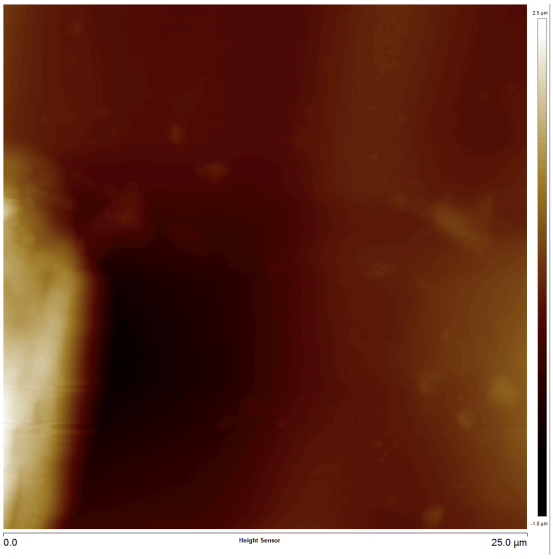
0.0
Height Sensor
25.0 µm

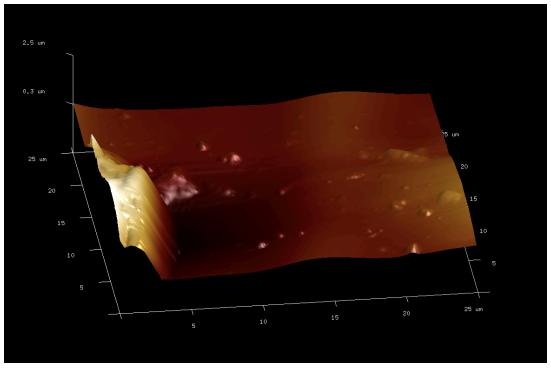

(9)

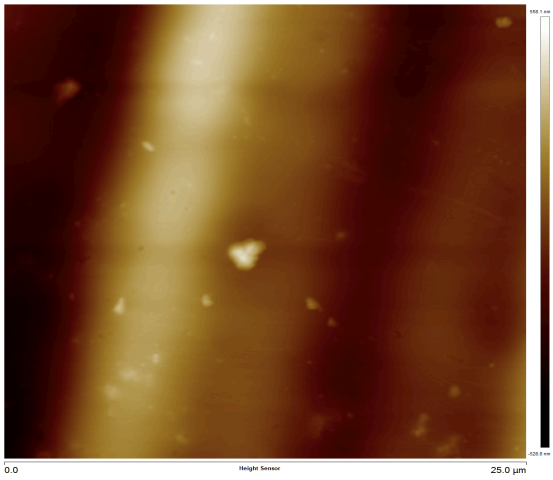

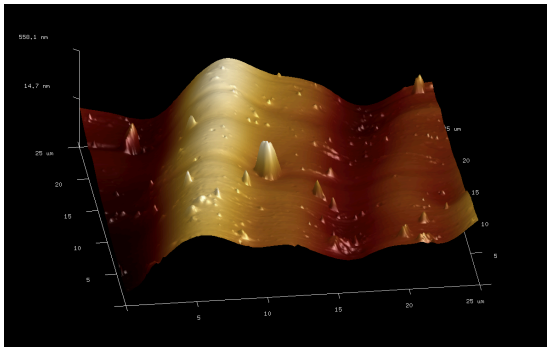

(10)

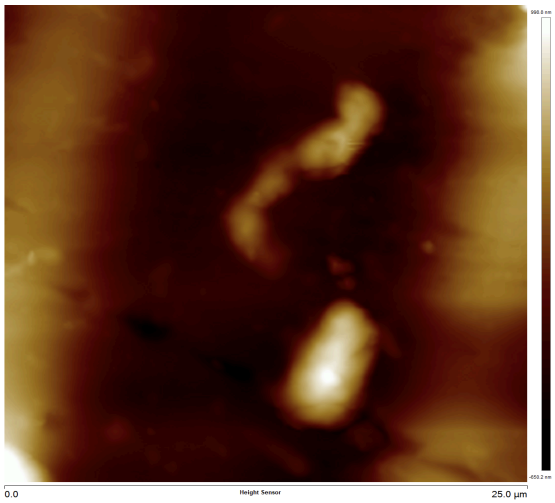

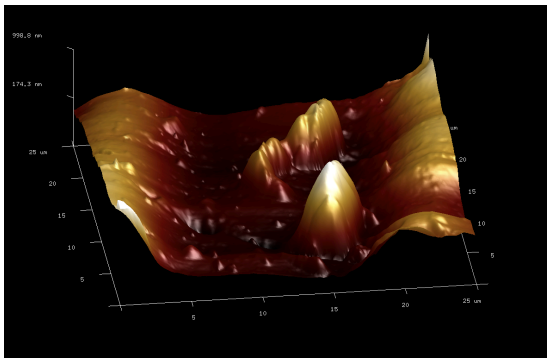

1000 Cycle Group

2D AFM Image **3D AFM Image**

(1)

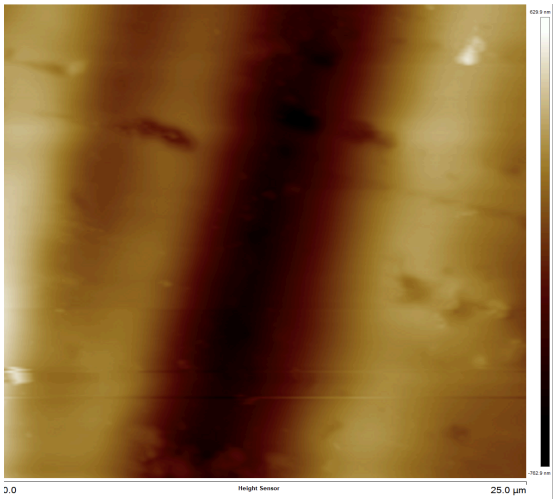

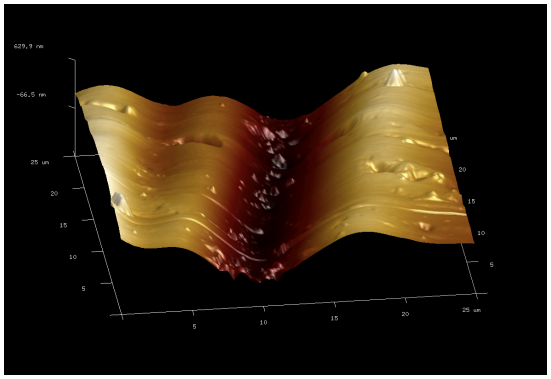

(2)

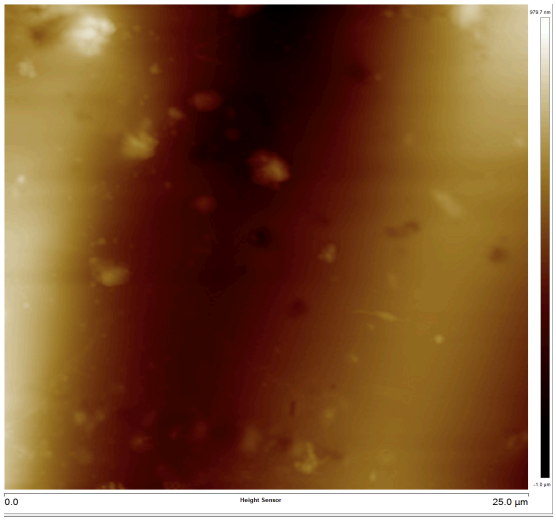
0.0
Height Sensor
25.0 µm

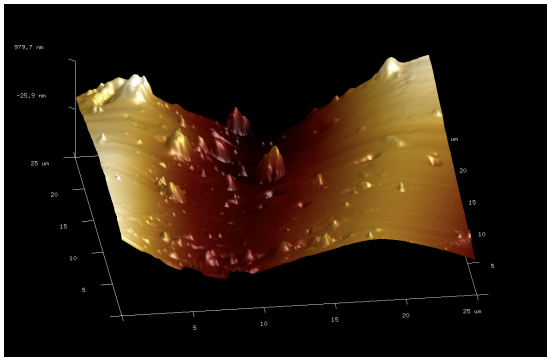

(3)

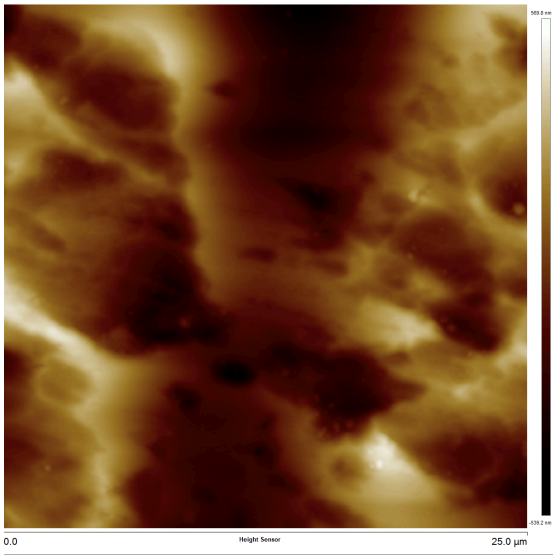
0.0
Height Sensor
25.0 µm

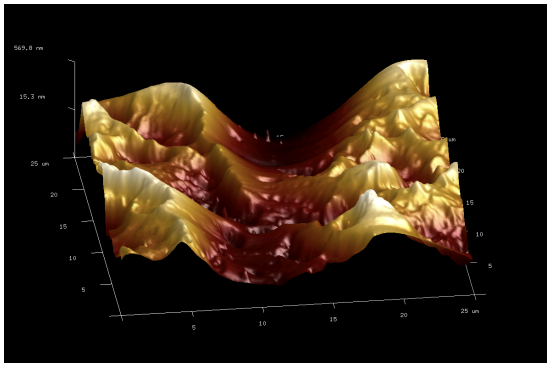

(4)

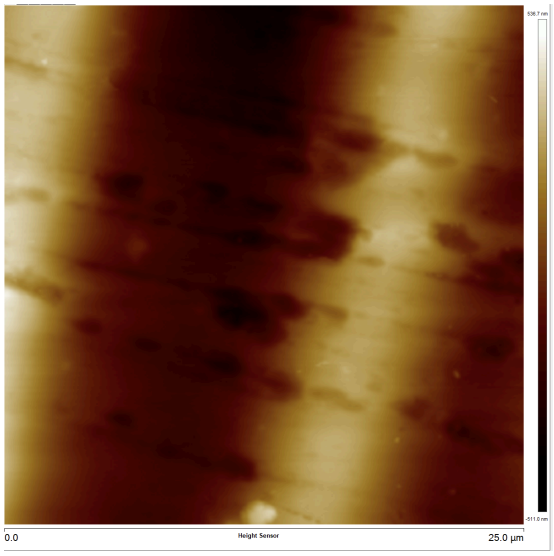
0.0
Height Sensor
25.0 µm

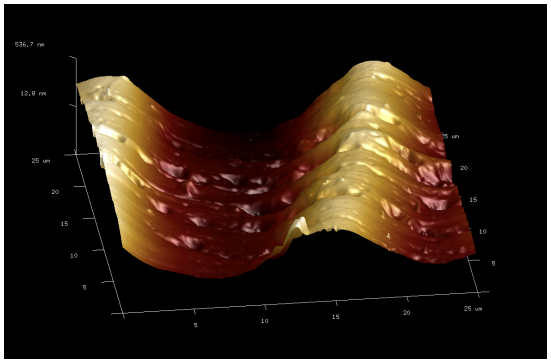

(5)

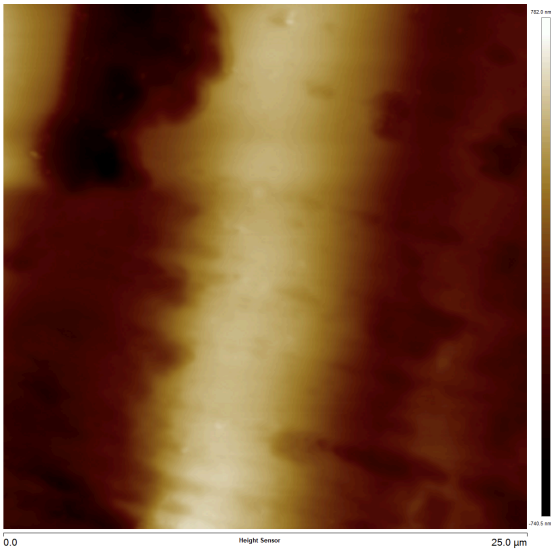
0.0
Height Sensor
25.0 µm

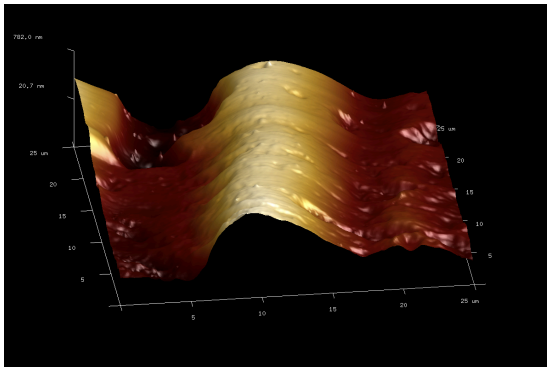
782.0 nm
20.7 nm
25 um
20
15
10
5
5
10
15
20
25 um

(6)

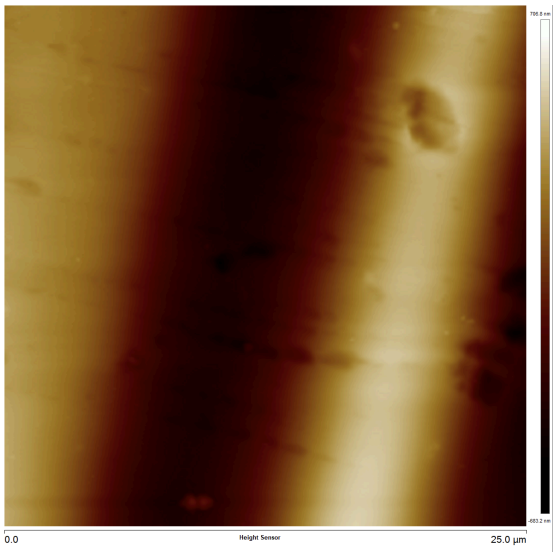
0.0
Height Sensor
25.0 µm

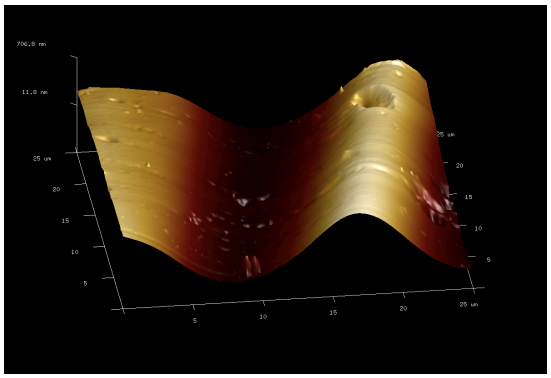
706.8 nm
11.8 nm
25 um
20
15
10
5
5
10
15
20
25 um

(7)

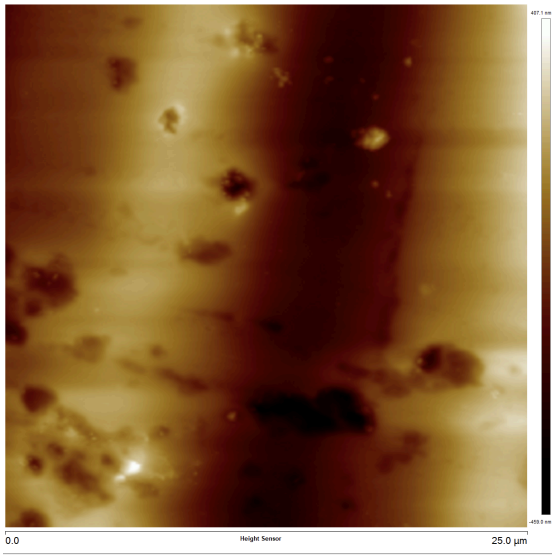
0.0
Height Sensor
25.0 µm

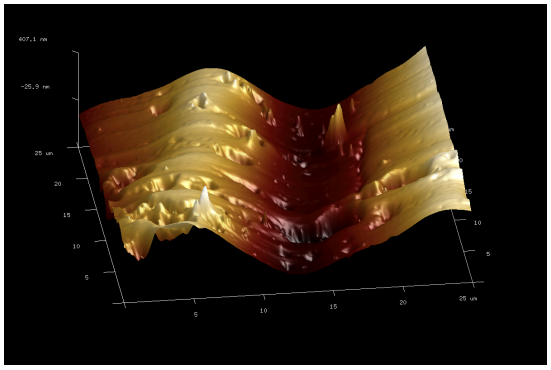
407.1 nm
-25.9 nm
25 um
20
15
10
5
5
10
15
20
25 um

(8)

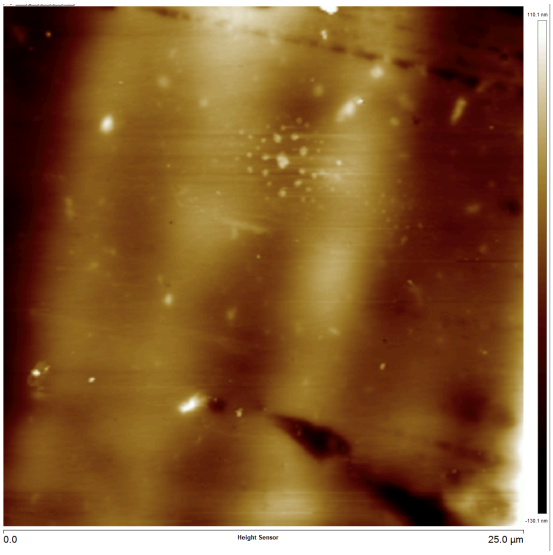
0.0
Height Sensor
25.0 µm

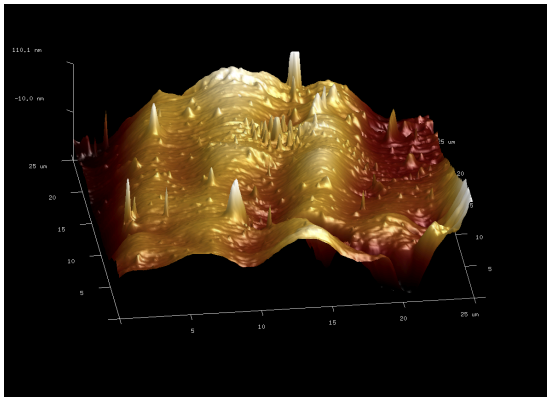

(9)

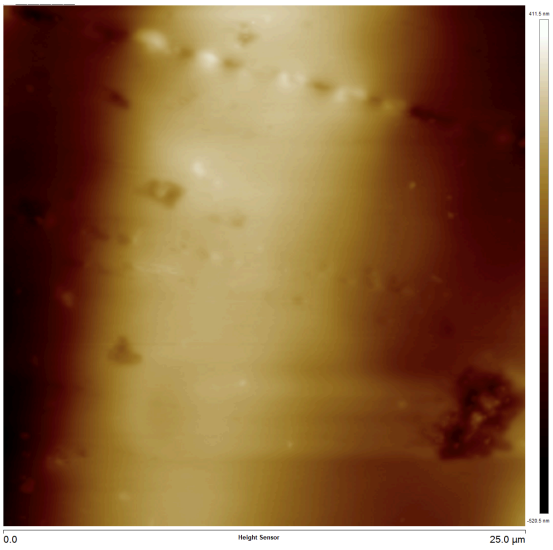
0.0
Height Sensor
25.0 µm

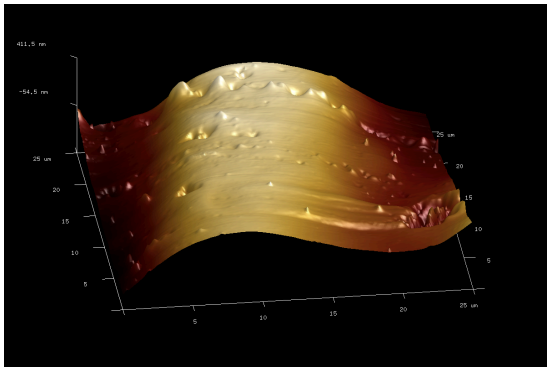

(10)

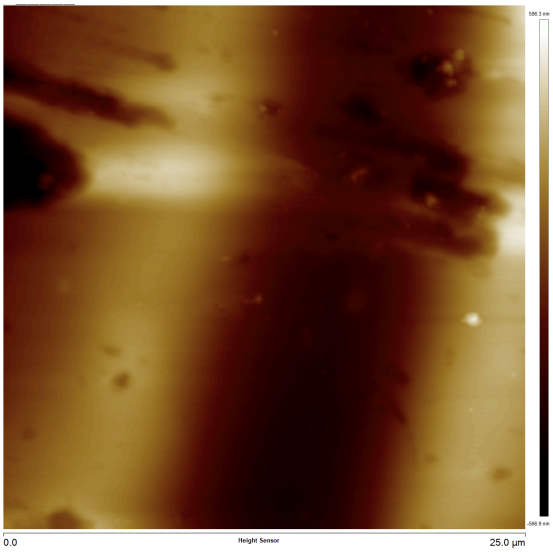
0.0
Height Sensor
25.0 µm

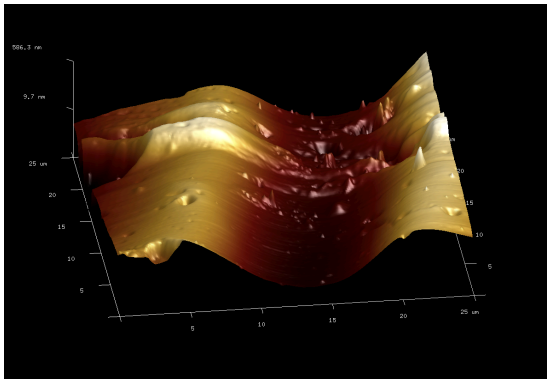

Appendix C: Display of Stress-Strain Curve

Control (No Fiber) - 1

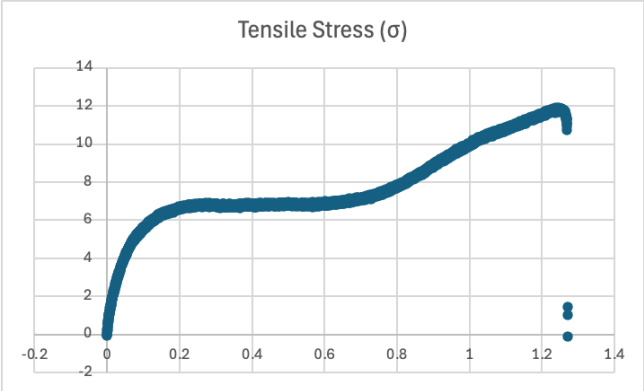

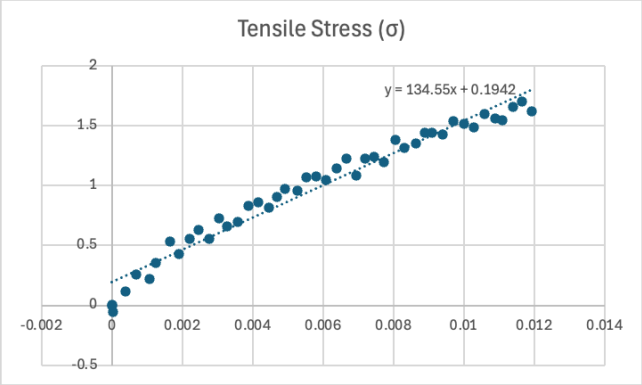

Control (No Fiber) - 2

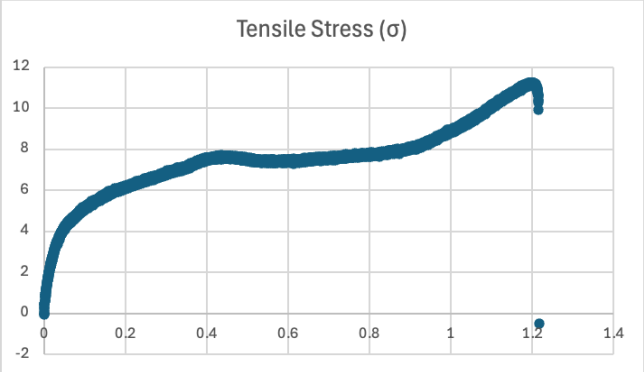

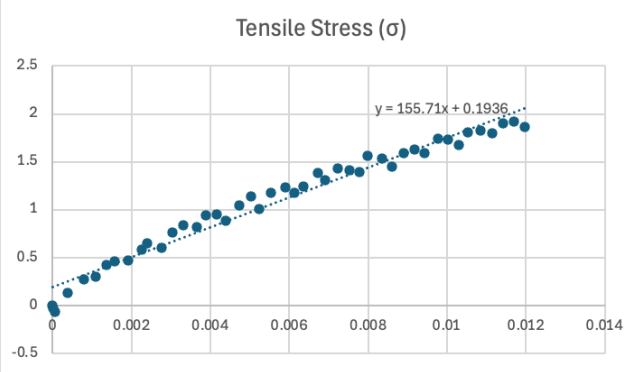

Control (No Fiber) - 3

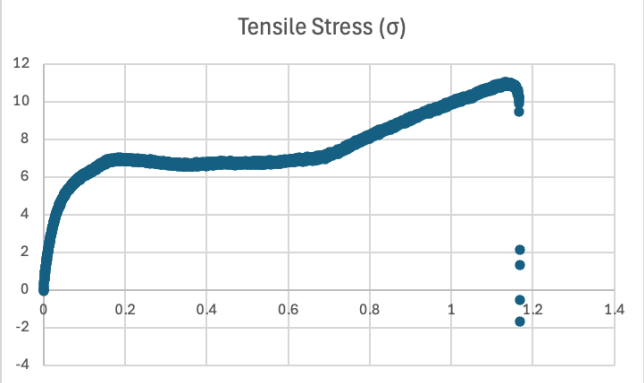

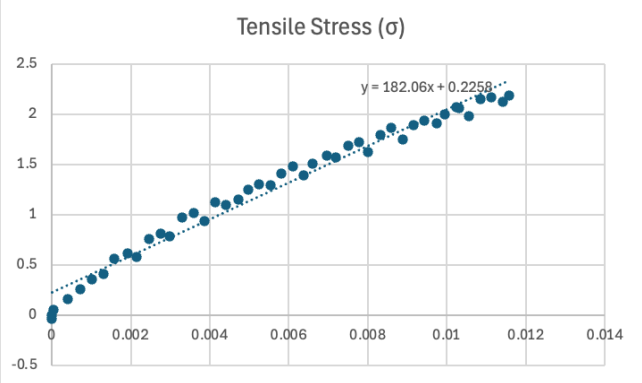

Control (No Fiber) - 4

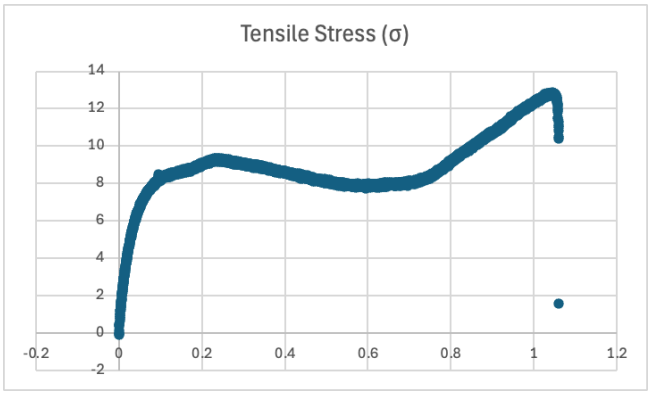

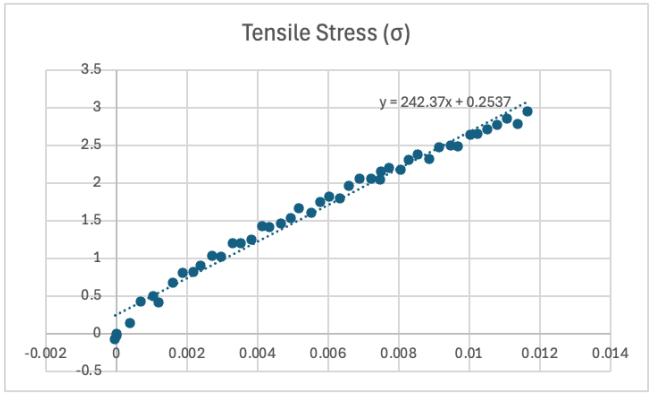

Control (Fiber) - 1

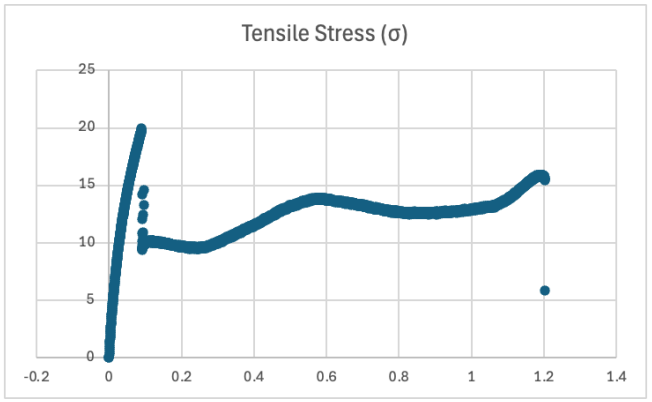

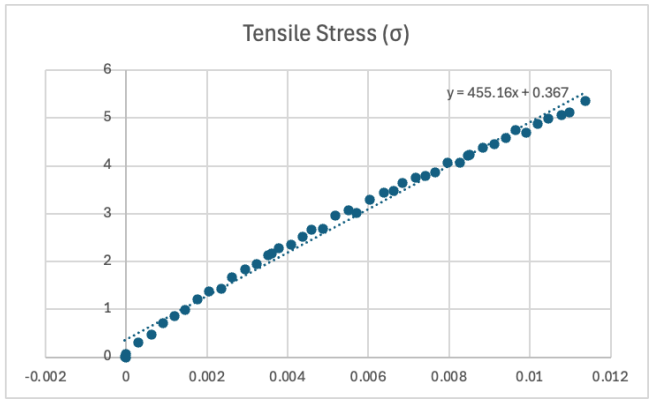

Control (Fiber) - 2

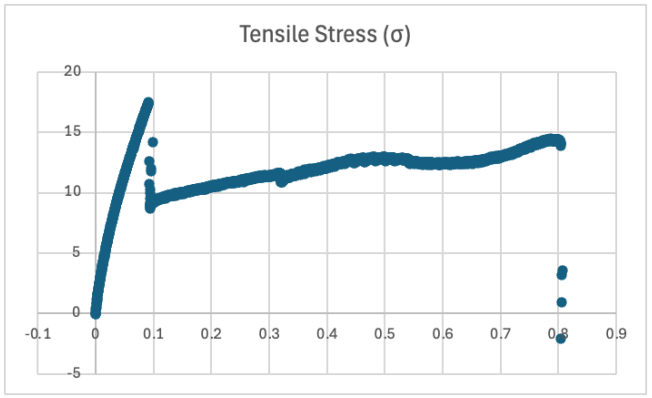

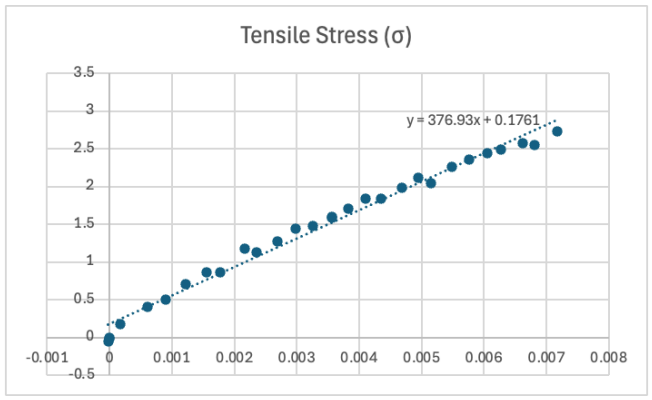

Control (Fiber) - 3

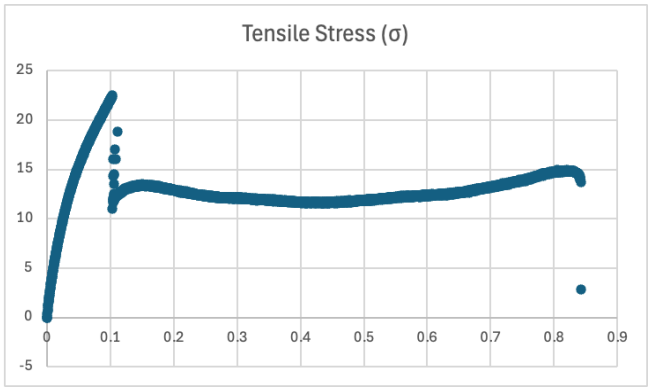

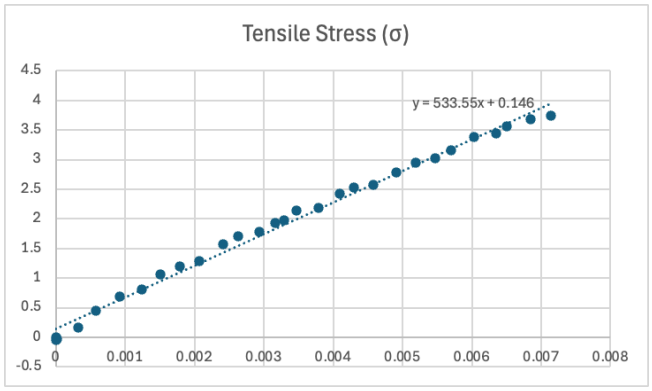

Control (Fiber) - 4

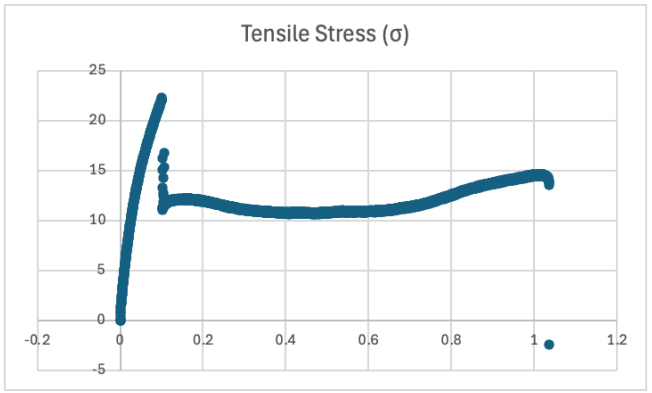

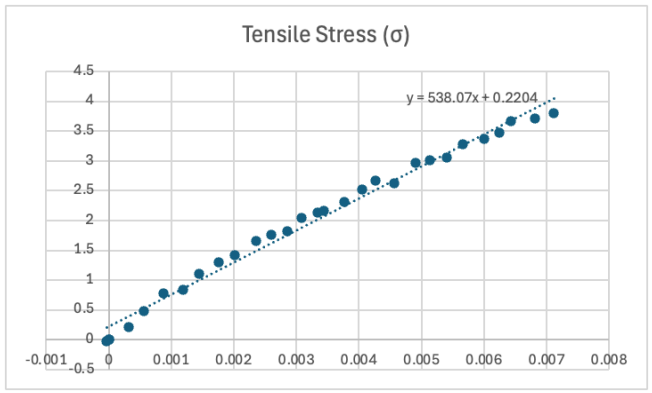

500 Cycle (No Fiber) - 1

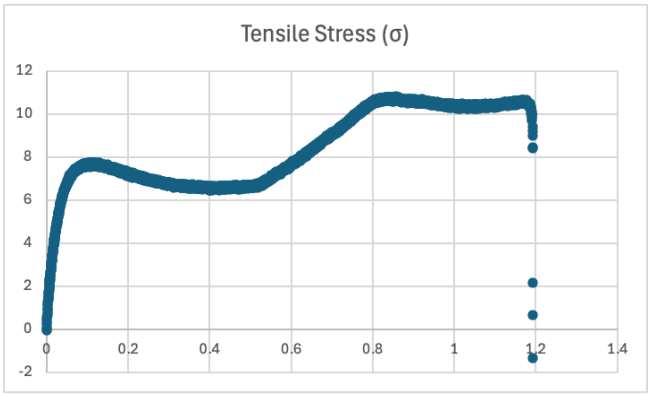

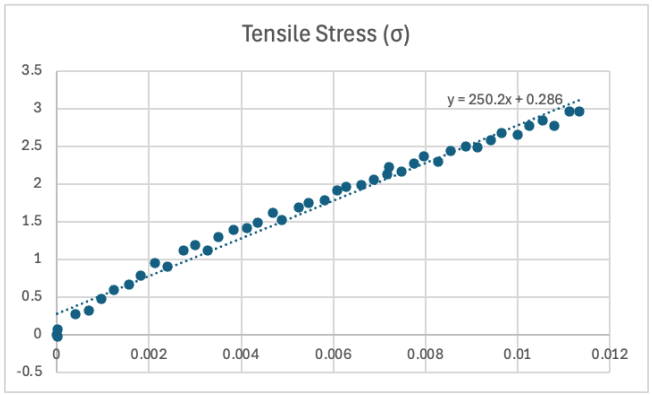

500 Cycle (No Fiber) - 2

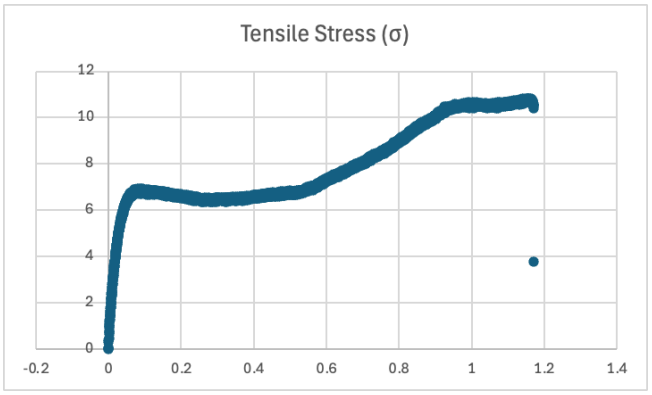

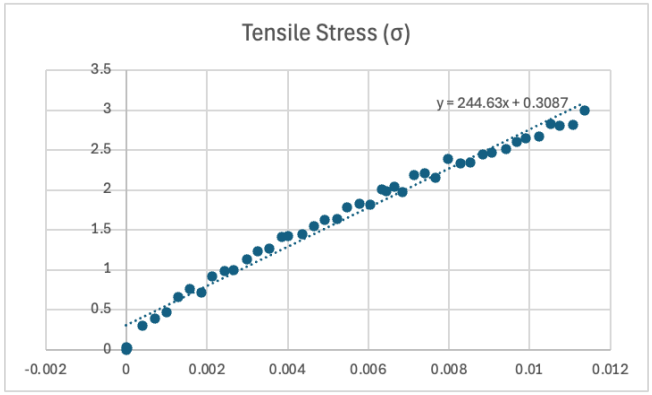

500 Cycle (No Fiber) - 3

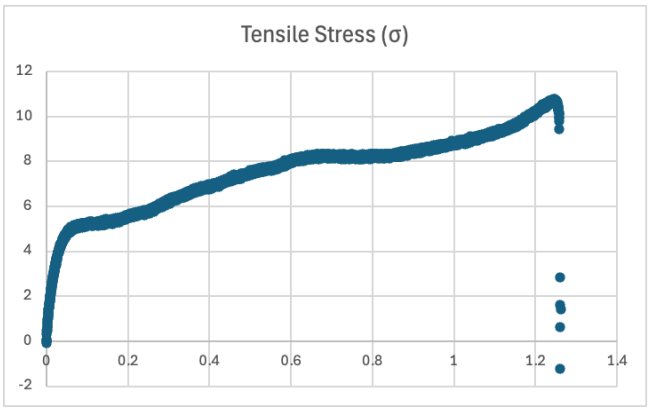

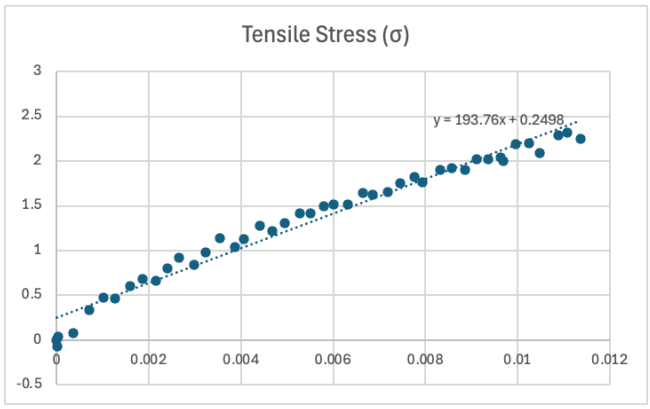

500 Cycle (No Fiber) - 4

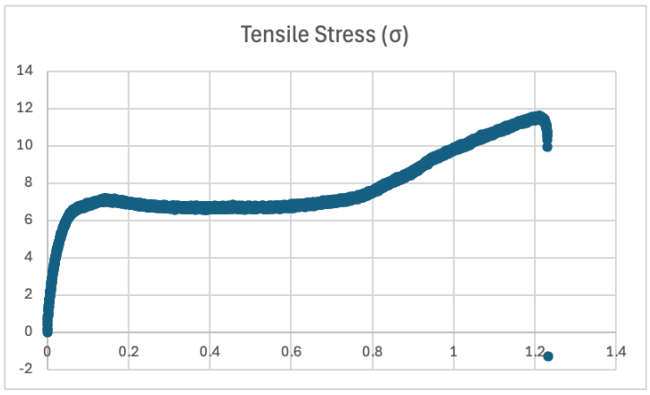

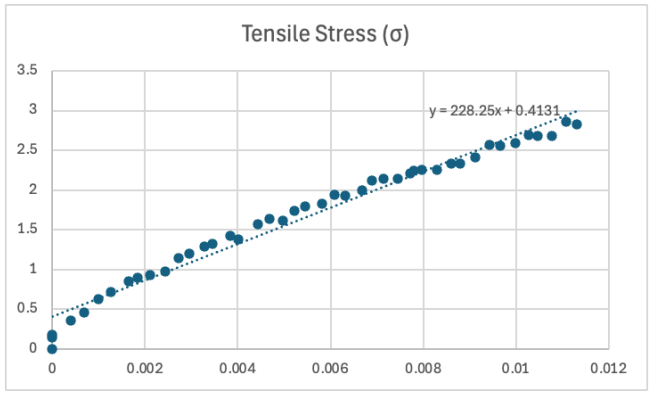

500 Cycle (Fiber) - 1

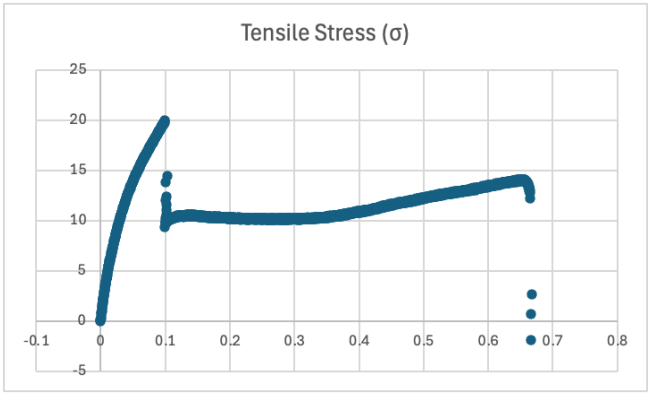

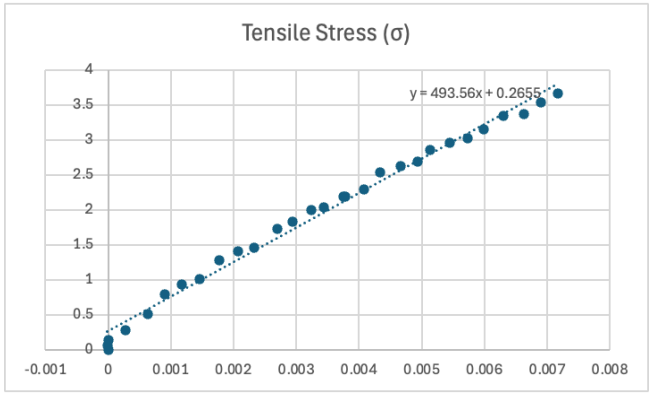

500 Cycle (Fiber) - 2

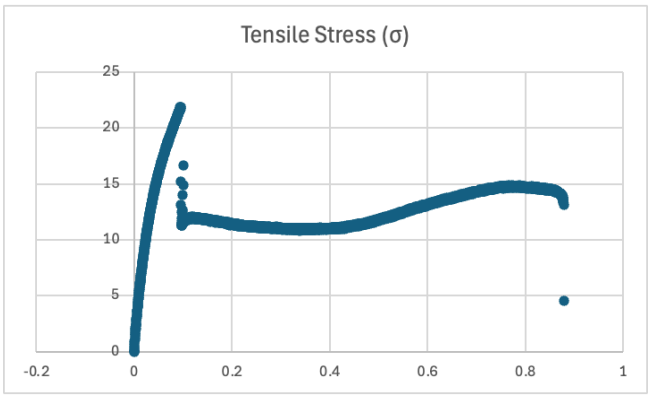

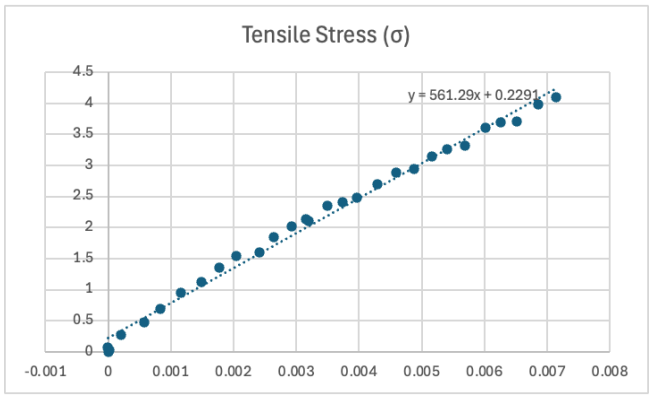

500 Cycle (Fiber) - 3

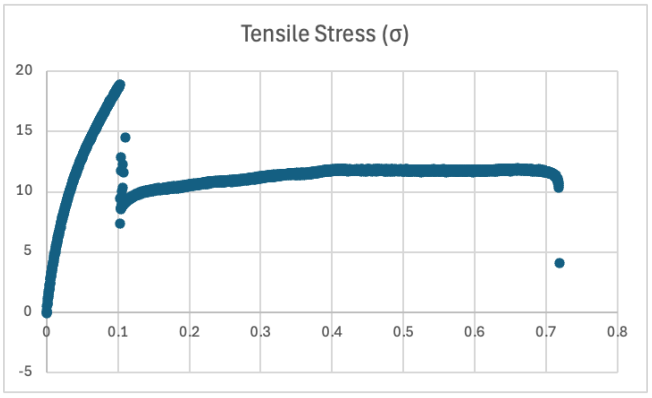

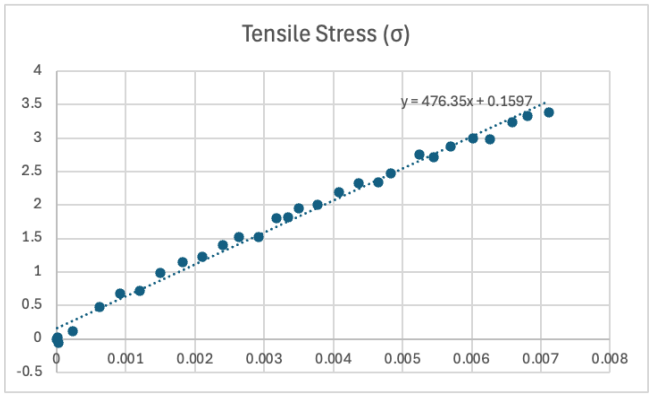

500 Cycle (Fiber) - 4

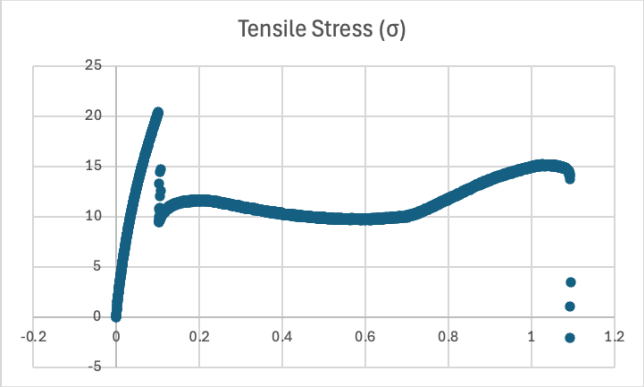

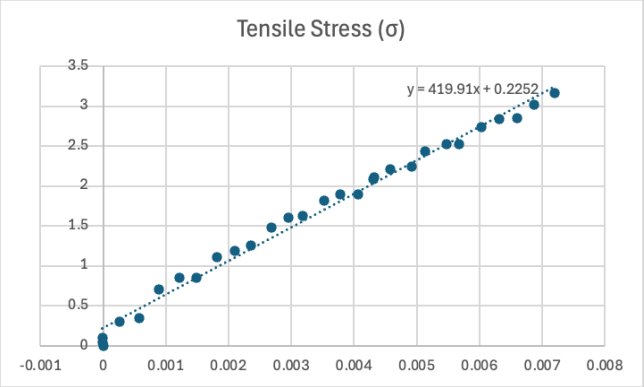

1000 Cycle (No Fiber) - 1

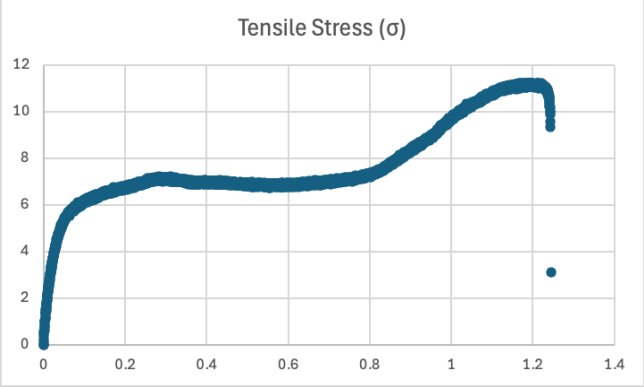

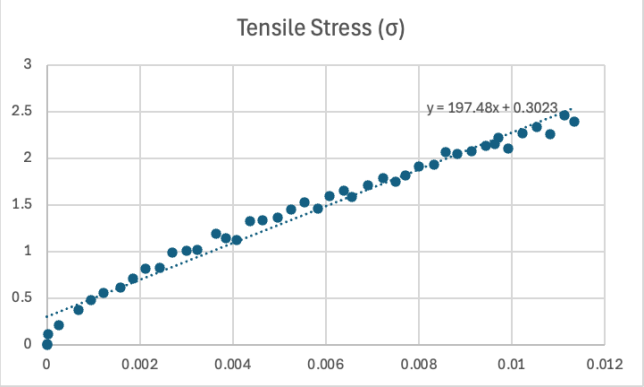

1000 Cycle (No Fiber) - 2

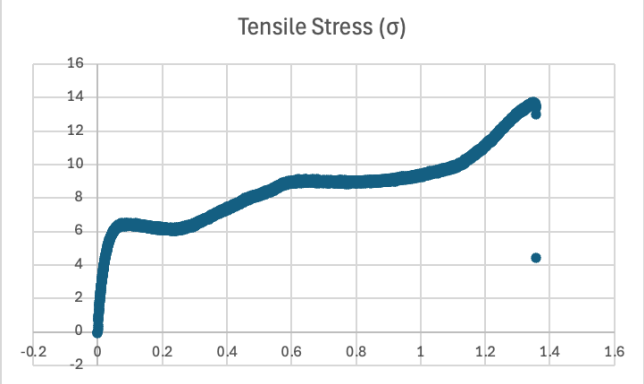

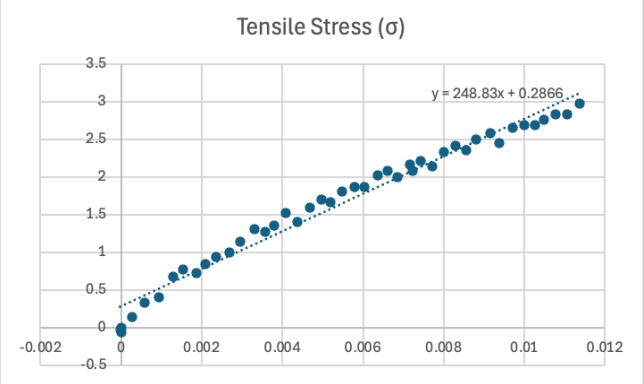

1000 Cycle (No Fiber) - 3

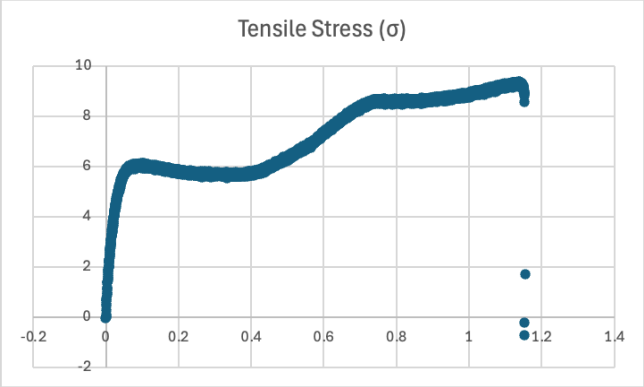

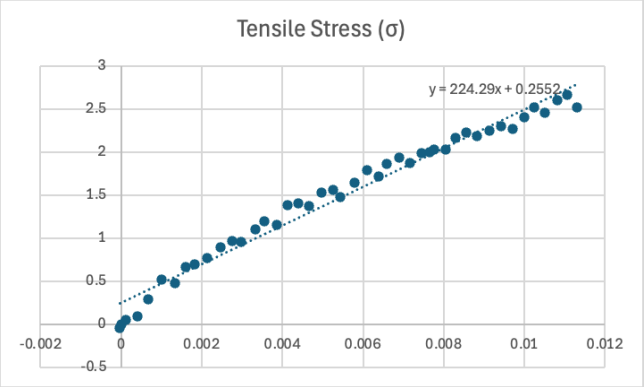

1000 Cycle (No Fiber) - 4

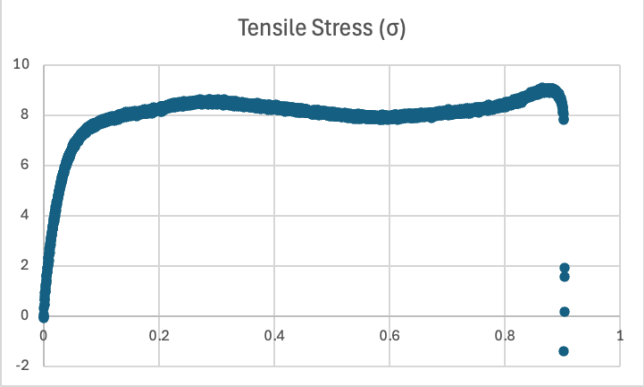

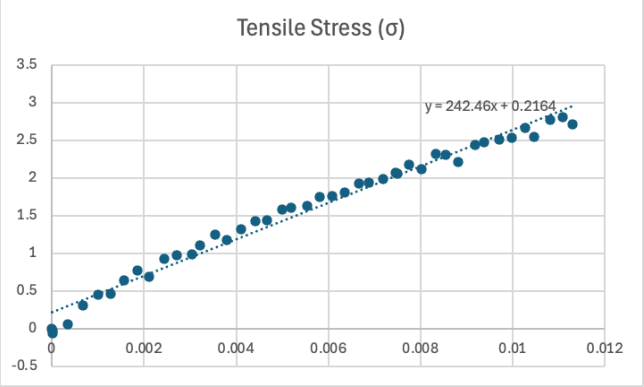

1000 Cycle (Fiber) - 1

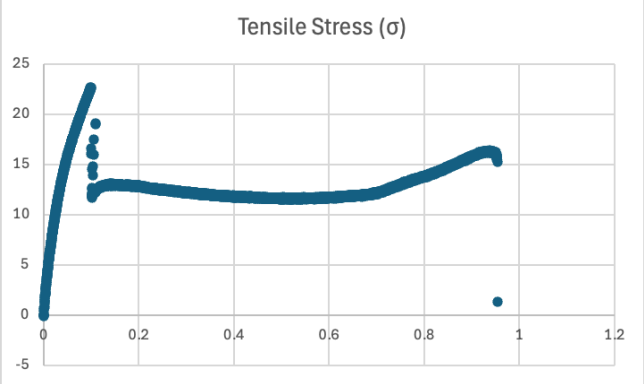

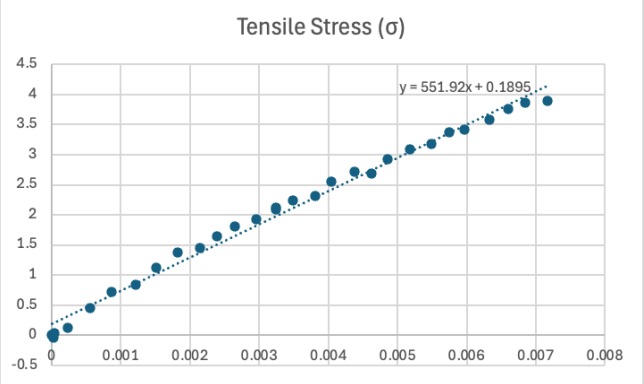

1000 Cycle (Fiber) - 2

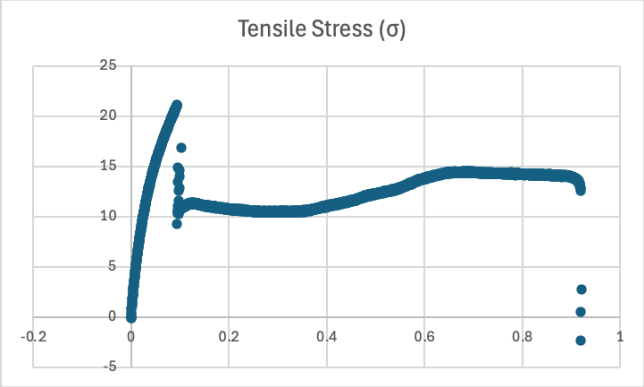

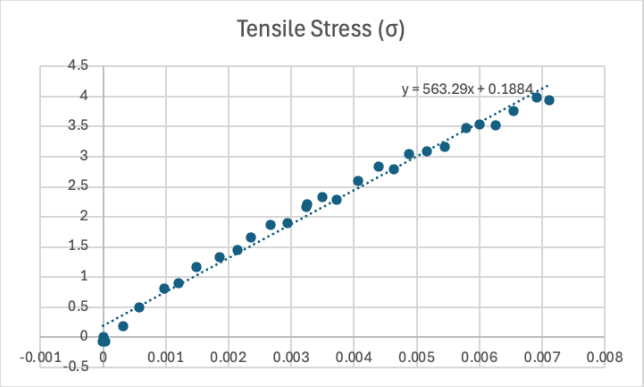

1000 Cycle (Fiber) - 3

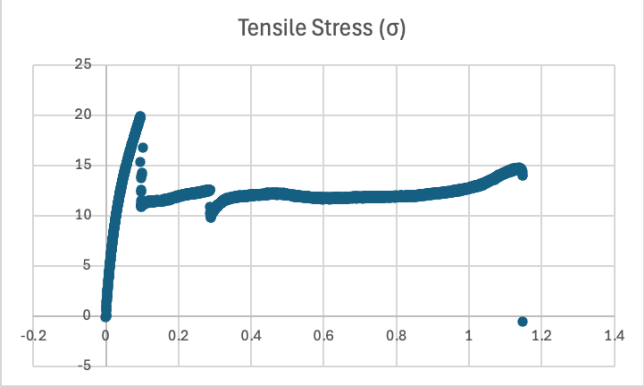

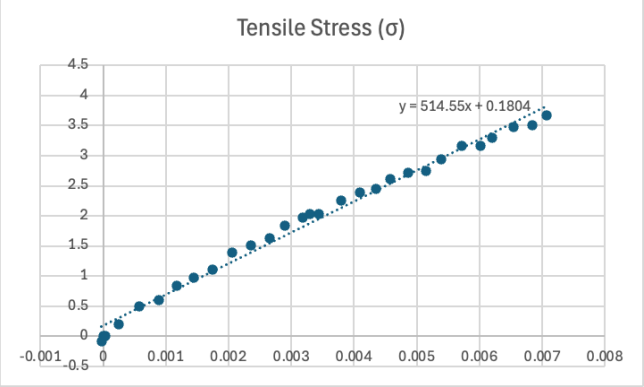

1000 Cycle (Fiber) - 4